Research Paper

PAIN®

OPEN

A peripheral CB_2 cannabinoid receptor mechanism suppresses chemotherapy-induced peripheral neuropathy: evidence from a CB_2 reporter mouse

Xiaoyan Lin[a], Zhili Xu[a], Lawrence Carey[a,b], Julian Romero[c], Alexandros Makriyannis[d], Cecilia J. Hillard[e], Elizabeth Ruggiero[f], Marilyn Dockum[f], George Houk[f], Ken Mackie[a,b,g], Phillip J. Albrecht[f], Frank L. Rice[f], Andrea G. Hohmann[a,b,g,*]

Abstract

CB_2 cannabinoid receptors (CB_2) are a promising therapeutic target that lacks unwanted side effects of CB_1 activation. However, the cell types expressing CB_2 that mediate these effects remain poorly understood. We used transgenic mice with CB_2 promoter–driven expression of enhanced green fluorescent protein (EGFP) to study cell types that express CB_2 and suppress neuropathic nociception in a mouse model of chemotherapy-induced peripheral neuropathy. Structurally distinct CB_2 agonists (AM1710 and LY2828360) suppressed paclitaxel-induced mechanical and cold allodynia in CB_2^{EGFP} reporter mice with established neuropathy. Antiallodynic effects of AM1710 were blocked by SR144528, a CB_2 antagonist with limited CNS penetration. Intraplantar AM1710 administration suppressed paclitaxel-induced neuropathic nociception in CB_2^{EGFP} but not CB_2 knockout mice, consistent with a local site of antiallodynic action. mRNA expression levels of the anti-inflammatory cytokine interleukin-10 were elevated in the lumbar spinal cord after intraplantar AM1710 injection along with the proinflammatory cytokine tumor necrosis factor alpha and chemokine monocyte chemoattractant protein-1. CB_2^{EGFP}, but not wildtype mice, exhibited anti-GFP immunoreactivity in the spleen. However, the anti-GFP signal was below the threshold for detection in the spinal cord and brain of either vehicle-treated or paclitaxel-treated CB_2^{EGFP} mice. EGFP fluorescence was coexpressed with CB_2 immunolabeling in stratified patterns among epidermal keratinocytes. EGFP fluorescence was also expressed in dendritic cells in the dermis, Langerhans cells in the epidermis, and Merkel cells. Quantification of the EGFP signal revealed that Langerhans cells were dynamically increased in the epidermis after paclitaxel treatment. Our studies implicate CB_2 expressed in previously unrecognized populations of skin cells as a potential target for suppressing chemotherapy-induced neuropathic nociception.

Keywords: CB_2 reporter mouse, Chemotherapy-induced peripheral neuropathy, CB_2 cannabinoid receptors, Peripheral analgesic mechanisms, Keratinocytes, Langerhans cells

1. Introduction

CB_1 and CB_2 are 2 major cannabinoid receptors in the endocannabinoid system.[60,66] Both receptors are implicated in pain physiology (for reviews, see Ref. 31, 35, 26, and 74). CB_1 is densely expressed in the central nervous system (CNS),[33,38,93] providing a neuroanatomical basis for CB_1-mediated psychotropic effects (for review see Ref. 65). By contrast, CB_2 is abundant in peripheral immune tissues such as spleen.[27,66,80] For CNS expression, CB_2 expression was detected in the diseased brain[9,10,23] but reportedly absent in the healthy brain,[13,27,29,53,66] although CB_2 mRNA was reported in low levels in scattered cell populations based on single cell RNAseq studies.[58,97] CB_2 protein and mRNA levels were increased in dorsal root ganglia (DRG) or spinal cord under conditions associated with neuropathic nociception.[7,8,90,95] After partial sciatic nerve ligation, CB_2 exhibited the highest signal in sciatic nerve macrophages while

Sponsorships or competing interests that may be relevant to content are disclosed at the end of this article.

[a] Psychological and Brain Sciences, Indiana University, Bloomington, IN, United States, [b] Program in Neuroscience, Indiana University, Bloomington, IN, United States, [g] Gill Center for Biomolecular Science, Indiana University, Bloomington, IN, United States, [c] Faculty of Experimental Sciences, Universidad Francisco de Vitoria, Madrid, Spain, [d] School of Pharmacy, Bouvé College of Health Sciences, Center for Drug Discovery, College of Science, Health Sciences Entrepreneurs, Northeastern University, Boston, MA, United States, [e] Department of Pharmacology and Toxicology, Neuroscience Research Center, Medical College of Wisconsin, Milwaukee, WI, United States, [f] Integrated Tissue Dynamics LLC, Rensselaer, NY, United States

**Corresponding author. Address: Department of Psychological and Brain Sciences, Indiana University, 1101 E 10th St, Bloomington, IN 47405-7007, United States. Tel.: +1 8128560672. E-mail address: hohmanna@indiana.edu (A.G. Hohmann).*

Supplemental digital content is available for this article. Direct URL citations appear in the printed text and are provided in the HTML and PDF versions of this article on the journal's Web site (www.painjournalonline.com).

PAIN 163 (2022) 834–851

http://dx.doi.org/10.1097/j.pain.0000000000002502

absent in neurons.[67] CB_2-selective agonists produce antinociceptive and anti-inflammatory effects without displaying cannabimimetic effects.[21,40,57] Thus, CB_2 offers a potentially advantageous profile compared with CB_1 as a therapeutic target.

Over the past decade, there have been more than 150 synthetic selective CB_2 agonists published patents.[2,64] Nevertheless, there has been limited success with CB_2 agonists in clinical trials.[64] Three synthetic CB_2 agonists are reported in clinic trials from ClinicalTrials.gov.[2,27] Despite extensive preclinical literature documenting that CB_2 activation produces antinociceptive and anti-inflammatory effects,[21,41,57] the cell types responsible for CB_2-mediated antiallodynic efficacy remain poorly understood, partially because of limited specificity of available CB_2 antibodies and low expression in CNS.[3] This gap in knowledge represents a barrier to development of mechanism-based analgesic drug development in humans.

In this study, we used a transgenic mouse with CB_2 promoter–driven expression of enhanced green fluorescent protein (CB_2^{EGFP})[55] to localize CB_2 and identify potential peripheral sites of antiallodynic efficacy. Paclitaxel was used to model chemotherapy-induced peripheral neuropathy (CIPN)[61] and is reported to reduce intraepidermal nerve fibers (IENFs).[12] Paclitaxel has adverse effects on cells undergoing proliferative replacement, including epidermal keratinocytes.[82] Keratinocytes, the most abundant cells in the skin, are in close contact with small-caliber sensory nerve endings and are implicated in nociception.[34] The presence of CB_2 in epidermal keratinocytes in the normal skin has been suggested using immunohistochemistry with CB_2 antibodies.[41,89]

We compared antiallodynic efficacy of CB_2 agonists (AM1710 and LY2828360) differing in their ability to penetrate the CNS in a model of paclitaxel-induced neuropathic nociception.[36,75] We confirmed peripheral mechanisms of CB_2-mediated antiallodynic efficacy using local injections in wildtype and CB_2 knockout mice and measured the impact of intraplantar agonist injection on mRNA expression levels of cytokines and chemokines in the lumbar spinal cord. Immunofluorescence consistent with CB_2 expression was observed in stratified patterns in epidermal keratinocytes and was altered by paclitaxel treatment in the hind paw skin from CB_2^{EGFP} mice. We observed CB_2 expression in Merkel cells and involvement of CB_2 in immunological responses involving dendritic and Langerhans cells (LCs). Our studies revealed previously unrecognized cell types that are dynamically regulated by paclitaxel treatment in the skin and support peripheral CB_2 mechanisms for suppressing CIPN.

2. Methods and materials

2.1. Animals

Adult male and female CB_2^{EGFP} reporter mice[55] bred at Indiana University on a C57BL/6J background, weighing 25 to 33 g, were used in this study. Adult CB_2KO mice (B6.129P2-CNR2 (tm1Dgen/J) on C57BL/6J background were bred at Indiana University. Animals were single housed 4 to 7 days before initiating pharmacological manipulations. All mice were maintained in a temperature-controlled facility (73 ± 2 ^{0}F, 45% humidity, 12-hour light or dark cycle, and lights on at 7 AM), with food and water provided ad libitum. All experimental procedures were approved by the Institutional Animal Care and Use Committee of Indiana University, Bloomington, and followed guidelines of the International Association for the Study of Pain.[99]

2.2. Drugs and chemicals

Paclitaxel (Tecoland Corporation, Irvine, California) was dissolved in a cremophor-based vehicle consisting of Cremophor EL (Sigma-Aldrich, St. Louis, Missouri), ethanol (Sigma-Aldrich), and 0.9% saline (Aqualite System; Hospira, Inc, Lake Forest, Illinois) at a ratio of 1:1:18 as previously published.[21] LY2828360 (8-(2-chlorophenyl)-2-methyl-6-(4-methylpiperazin-1-yl)-9-(tetrahydro-2H-pyran-4-yl)-9H-purine) (Sai, Inc, Kolkata, India) was dissolved in a vehicle containing 10% of dimethyl sulfoxide (Sigma-Aldrich) and ALKAMULS EL-620 (Rhodia, Cranbury, NJ), ethanol, and saline at a ratio of 1:1:18. SR144528 (SR2) (5-(4-chloro-3-methylphenyl)-1-(4-methylbenzyl)-N-(1, 3, 3-trimethylbicyclo [2.2.1] heptan-2-yl)-1H-pyrazole-3-carboxamide) was provided by the NIDA Drug Supply Program (RTI, Research Triangle Park, North Carolina). AM1710 (synthesized in the laboratory of A.M. at Northeastern University, Boston, Massachusetts) and SR144528 were dissolved in vehicle, 5:2:2:16 ratio of dimethyl sulfoxide, ALKAMULS EL-620, ethanol, and saline.

2.3. General experimental protocol

In all studies, the experimenter was blinded to the treatment condition and mice were randomly assigned to experimental conditions. Treatment groups were separated into multiple cohorts; each cohort contained multiple groups and testing of the different cohorts overlapped. Paclitaxel was administered by intraperitoneal (i.p.) injection 4 times on alternate days (ie, 4 mg/kg i.p. on day 0, 2, 4, and 6 (approximately 48 hours between injections); cumulative dose 16 mg/kg) to produce a CIPN condition, as described previously.[14,19,21,42,48–50,52,54,83–88] Control mice received an equal volume of cremophor-based vehicle on the same treatment schedule. Development of paclitaxel-induced allodynia was assessed on day 0, 4, 7, 11, and 14. Injections were always performed after the behavioral assessment when these events occurred on the same day (ie, day 0 and day 4).

Effects of pharmacological manipulations were assessed 30 minutes after drug or vehicle administration during the maintenance phase of paclitaxel-induced neuropathy (ie, beginning day 18-20 after initial paclitaxel injection or as indicated).

In experiment 1, we evaluated whether CB_2^{EGFP} mice of both sexes develop mechanical and cold allodynia in response to treatment with paclitaxel or its vehicle (n = 6 per group). In experiment 2, we compared the antiallodynic efficacy of 2 structurally distinct CB_2 agonists that differ in their ability to penetrate the CNS (ie, starting on day 18 after initial paclitaxel injection; n = 10-11/group). Male and female mice were given i.p. injections of either AM1710, a CB_2 agonist with limited CNS penetration,[75] or LY2828360, a CNS-penetrant CB_2 agonist that failed in a Phase 2 clinical trial for osteoarthritis treatment but has been shown to be safe in people.[54,69] We evaluated the dose response of AM1710 (1, 3, 5, and 10 mg/kg i.p.) and LY2828360 (0.1, 0.3, 1, 3, 5, and 10 mg/kg i.p.) in producing antiallodynic efficacy using a within-subjects escalating dosing paradigm. Successive doses were separated by 2 to 4 days. In experiment 3, we tested for peripheral antinociceptive mechanisms in male and female CB_2^{EGFP} mice (n = 7-8/group) starting on day 18 after initial paclitaxel injection. Our previous study suggested that unlike Δ^9-THC or CP55,940, AM1710 does not produce tolerance or physical dependence after 8 days of chronic treatment.[19,21] The dose which produced maximal antiallodynic efficacy in the dose response analysis (experiment 2) was selected for chronic dosing. In this article, we evaluated whether repeated systemic administration of AM1710 (5 mg/kg/day i.p. × 8 days)[21] suppressed paclitaxel-induced neuropathic nociception in a manner that was susceptible to blockade by SR144528 (2.1 mg/kg/day, i.p), a CB_2 antagonist with limited CNS penetration.[11]

In experiment 4, a separate study was performed to further evaluate a peripheral site of antialloydnic efficacy in paclitaxel-treated mice. Male CB_2^{EGFP} or male CB_2KO mice received

AM1710 injected locally in the paw using a direct intraplantar (i.pl.) injection (ie, day 18 after initial paclitaxel or cremophor-vehicle injection (n = 6-10/group). Mice were given a single i.pl. injection of AM1710 (30 μg in 10 μL volume) or vehicle (identical volume) into the right hind paw. Withdrawal responses evoked by mechanical or cold stimulation were measured in hind paws ipsilateral and contralateral to the side of injection 30 minutes after drug injection as indicated. Tissue derived from separate cohorts of paclitaxel-treated mice receiving identical treatments were used in reverse transcription polymerase chain reaction (RT-PCR) analysis (described below).

2.4. Assessment of mechanical allodynia

In experiments 1 to 4, paw withdrawal thresholds (g) to mechanical stimulation were measured in duplicate for each paw through an electronic von Frey anesthesiometer (IITC model Alemo 2390–5, IITC Life Science, Woodland Hills, CA) as described previously.[21,49,52,54,88] Mice were placed on an elevated metal mesh table and allowed to habituate under individual, inverted plastic cages to the testing platform for at least 20 minutes until exploratory behavior ceased. After the habituation period, a force was applied continuously to the midplantar region of the hind paw until a paw withdrawal response was elicited; the force was applied using a single, semiflexible tip (0.8 mm diameter) connected to the anesthesiometer to deliver a uniform surface area of stimulation at all applied forces. Mechanical stimulation was terminated when the animal withdrew its paw and the value of the applied force was automatically recorded in grams (g) by a digital display. Mechanical paw withdrawal thresholds were obtained in duplicate for each paw and are reported as the mean of duplicate determinations (ie, averaged across paws or as indicated) from each animal, with one exception. In studies using unilateral i.pl. injections of drug or vehicle, responses are reported separately for the ipsilateral (injected) and contralateral (noninjected) paws. Behavioral data show means of a single determination per animal, averaged across animals (not across stimulations) for each treatment group in all studies.

2.5. Assessment of cold allodynia

In experiments 1 to 4, responsiveness to cold was assessed using the acetone method in the same mice used to assess responsiveness to mechanical stimulation.[21,49,52,54,88] Mice were allowed at least 20 minutes to habituate to the chamber before testing. An acetone (Sigma-Aldrich) bubble (approximately 5-6 μL) formed at the end of a blunt one C.C. syringe hub was gently applied to the plantar surface of the hind paw through the floor of the mesh platform. Care was taken to avoid mechanical stimulation to the hind paw with the syringe itself. Response time (seconds) spent attending to (ie, elevating, licking, biting, or shaking) the paw stimulated with acetone was measured in triplicate for each paw to assess cold allodynia as previously published by our group.[21,49,52,54,88] The total time the animal spent attending to the acetone-stimulated paw (ie, elevation, shaking, or licking) was recorded over 1 minute after acetone application. Acetone was applied 3 times to each paw with a 3-minute interval between applications. Values for each animal were calculated as described above for responses to mechanical stimulation.

2.6. RNA isolation and reverse transcriptase quantitative polymerase chain reaction for CB_2, green fluorescent protein, and cytokines mRNA

Real-time (RT) quantitative PCR (qPCR) was used to examine the distribution of CB_2 and GFP mRNAs in the spleen, lumbar spinal cord, and paw skin tissues in CB_2^{EGFP} mice. As a control, tissues derived from wild type mice were processed and quantified concurrently (n = 7-9/group, mixed sex). We also compared CB_2 and GFP mRNA expression levels in the spleen, lumbar spinal cord, and paw skin derived from paclitaxel and cremophor vehicle–treated CB_2^{EGFP} mice. CB_2^{EGFP} mice received paclitaxel or its cremophor-based vehicle (n = 6-8/group, mixed sex) as described previously[21] and were euthanized on day 16 after the onset of paclitaxel or vehicle treatments when behavioral signs of neuropathic nociception were maximal and stable. Mice were deeply anesthetized with isoflurane and then transcardially perfused with Hanks balanced salt solution.

To examine the impact of peripheral cannabinoid antiallodynic mechanisms on proinflammatory cytokine and chemokine mRNA expression levels, paclitaxel-treated CB_2^{EGFP} reporter mice (male and female, n = 6-7/group) received local injections of either AM1710 (30 μg, i.pl.) or an equivalent volume of vehicle during the maintenance phase of paclitaxel-induced neuropathic nociception. Paclitaxel-treated mice received a unilateral local injection of AM1710 (30 μg, i.pl.) or vehicle on day 16 after initial paclitaxel treatment. At 45 minutes after the injections, animals were deeply anaesthetized with isoflurane, euthanized by decapitation, and the lumbar (L4-L5) region of the spinal cord rapidly dissected and frozen (−80°C) until use in mRNA assessments. Reverse transcriptase qPCR methods were used to measure mRNA expression levels of anti-inflammatory interleukin 10 (IL-10) or proinflammatory (tumor necrosis factor alpha [TNF-α], IL-6, and IL-1β) cytokines or chemokine monocyte chemoattractant protein (MCP-1).

In all studies, total RNA was purified using TRIzol (Thermo Fisher, Waltham, MA) and RNeasy mini kit from the tissue samples according to the manufacturer's manual. Quantification of total mRNA was assessed using a NanoDrop 2000C UV-Vis spectrophotometer at 260 nm. One-step reverse transcriptase qPCR was performed using the Thermo Fisher Scientific Power SYBR Green RNA to C_T^{TM} 1–Step for a total volume of 10 μL and a template concentration of 50 ng/μL according to the manufacturer's recommendations. Thermal cycle conditions were 48°C for 30 minutes (reverse transcription step), 95°C for 10 minutes, followed by 40 cycles of 95°C for 15 seconds, and 60°C for 1 minute. A melting curve analysis was performed at 95°C for 15 seconds, 60°C for 1 minute, and 95°C for 15 seconds after every run to ensure a single sharp amplified product for every reaction. All reactions were performed in duplicate in 384-well reaction plates (Thermo Fisher Scientific). The mRNA expression levels were expressed as relative quantities to control and calculated by $2^{(-\Delta\Delta Ct)}$ method where glyceraldehyde 3-phosphate dehydrogenase (GAPDH) was used as housekeeping reference gene. Primer sequences are listed as following:

GAPDH Sense: 5′-GGGAAGCTCACTGGCATGGC-3′ Anti-sense: 5′-GGTCCACCACCCTGTTGCT-3′; MCP1 Sense: 5′-GAAGGAATGGGTCCAGACAT-3′ Anti-sense: 5′-ACGGGT-CAACTTCACATTCA-3′; IL6 Sense: 5′-GCCTTCTTGGGACT-GATGCT-3′ Anti-sense: 5′-TGCCATTGCACAACTCTTTTC-3′; TNFα Sense: 5′-CGTCGTAGCAAACCACCAAG-3′ Anti-sense: 5′TAGCAAATCGGCTGACGGTG-3′; IL-1beta Sense: 5′-CGTGGACCTTCCAGGATGAG-3′.

Anti-sense: 5′-CATCTCGGAGCCTGTAGTGC-3′; IL10 Sense: 5′ GGACTTTAAGGGTTACTTGGGTTGCC-3′ Anti-sense: 5′CATTTTGATCATCATGTATGCTTCT-3′; CB_2 Sense: 5′- CTCGGTTACAGAAACAGAGGCTGATGTG -3′ Anti-sense: 5′- TCTCTCTTCGAGGGAGTGAACTGAACG-3′; eGFP sense: 5′- ACATGGTCCTGCTGGAGTTCGTGAC -3′ Anti-sense: 5′-CTCTTCGAGGGAGTGAACTGAACGG -3′.

2.7. Tissue preparation for immunohistochemistry

Male and female CB_2^{EGFP} mice receiving paclitaxel (4 mg/kg, i.p. on day 0, 2, 4, and 6) or its cremophor-based vehicle (identically time/volume dosed) were euthanized on day 16 after the onset of paclitaxel or vehicle treatments. Mice were deeply anesthetized with isoflurane and then transcardially perfused with 0.1% heparinized 0.1 M phosphate-buffered saline (PBS) followed by ice cold 4% paraformaldehyde. Spleen, lumbar spinal cord, and brain were extracted and kept in the same fixative for 24 hours, then cryoprotected in 30% sucrose for 3 days before sectioning. Brains, spleens, and spinal cords were sectioned (30 μm thickness) with a cryostat and maintained in an antifreeze solution (50% sucrose in ethylene glycol and 0.1 M PBS) before immunolabeling. Free floating sections were washed in 0.1 M PBS, blocked with buffer consisting of 5% donkey serum and 0.1% Triton X-100 in 0.1 M PBS, then incubated overnight in goat polyclonal antibody to GFP (AB0020-200, 1:1000; Sicgen, Cantenhede, Portugal) at 4°C. Sections were then incubated in donkey anti-goat AlexaFluor 594 (1:500, Thermo Fisher), stained with 4',6-diamidino-2-phenylindole (DAPI) (0.1 μg/mL), and treated with Sudan black B (0.2% wt/vol, Sigma Aldrich, St Louis, MO) to quench autofluorescence in CNS tissues.

To detect whether immunofluorescence was present in hind paw epidermal tissue, adult CB_2^{EGFP} reporter mice were deeply anesthetized and sacrificed by transcardial perfusion with 0.1 M PBS, followed by 4% paraformaldehyde in 0.1 M PBS at pH 7.4 at 4°C. Male and female CB_2^{EGFP} mice received paclitaxel (4 mg/kg, i.p. on day 0, 2, 4, and 6) or its cremophor-based vehicle (with identical time or volume dosing) and were euthanized on day 16 after the onset of paclitaxel or vehicle treatments.

Both hind paws from each mouse were dissected, postfixed at 4°C in the perfusion fixative for 4 hours, stored in PBS-azide at 4°C, and subsequently shipped cold overnight to Integrated Tissue Dynamics, LLC, for immunohistochemical processing. Glabrous hind paw skin was dissected free, cryoprotected in 30% sucrose in PBS overnight at 4°C, snap frozen, and sectioned at 14 μm on a cryostat in a plane perpendicular to the skin surface and parallel to the long axis of the foot. Serial sections were mounted over alternating slides and air dried overnight. Two alternating slides for each specimen were processed for immunolabeling with a rabbit anti-GFP primary antibody (1:400, Cell Signaling 2555; Cell Signaling Technology, Danvers, MA). One slide was subsequently prepared with secondary anti-rabbit Alexa 488 (1:250, Life Technologies A21206; Life Technologies, Carlsbad, CA) to augment the endogenous green EGFP fluorescence. The other slide was processed with secondary anti-rabbit Cy3 (1:500, Jackson ImmunoResearch, 711-165-152; Jackson ImmunoResearch, West Grove, PA) for red fluorescence detection of EGFP protein as distinct from EGFP green fluorescence. These methods and controls were documented previously.[96] Two additional slides of alternating sections were prepared for Cy3 visualization. One was processed with a polyclonal rabbit anti-CB_2 primary antibody raised against the 1 to 32 amino acid sequence of the rat N-terminus domain that has been well documented to cross-react with mouse (Abcam Ab3561 1:200; Abcam, Cambridge, United Kingdom). The other slide was processed with a rabbit polyclonal antibody raised against human protein gene product 9.5 (PGP; 1:800 Cedarlane RA95101; Cedarlane Laboratories, Burlington, NC) that is the designation for a phylogenetically conserved enzyme (ubiquitin C-terminal hydrolase L1, UCHL1) that is robustly expressed by all types of peripheral innervation.

2.8. Digital imaging and microscopy

Spleen, lumbar spinal cord, and brain images were captured using a Leica DM6B microscope equipped with a Leica DFC9000 GT camera and Leica Application Suite X software (Leica Microsystems, Wetzlar, Germany).

Epifluorescence images from mouse volar pads were captured using an Olympus BX51-WI microscope equipped with a Hamamatsu ER, DVC high-speed camera, 10 position LEP motorized filter wheel with standard fluorescent filter sets for delineating red or blue or green fluors, 3-axis motorized stage system, linear focus encoder, and Vistek vibration isolation platform (MBF Bioscience, Williston, VT). Image capture settings were the same for all Cy3-labeled specimens as based on prior publication.[96] For anti-GFP Alexa-488 imaging, capture settings were also standardized based on prior Alexa-488 publication.[96] For these preparations, the same camera setting was used to capture endogenous EGFP green fluorescence before being processed and subsequently reimaged for anti-GFP Alexa-488. The same green channel setting was also used to capture endogenous EGFP green fluorescence in preparations double labeled with anti-GFP and anti- CB_2 processed for Cy3 red fluorescence.

The structure and biochemistry of the skin, especially the epidermis, varies depending on different physical stressors that are related to varied locations on the body surface. Therefore, the analyses were standardized to 3 regions passing longitudinally through the volar pads on the lateral halves of the glabrous hind paw.[41] These are consistently predictable, pronounced pads located at the base of the digits and in distal to proximal locations along the medial and lateral margins of the foot, which are the primary points of contact and weight bearing with the ground. The sectioning orientation passes longitudinally through these pads enabling a selection of those locations in the sections that are near the apex of the pads.

Neurolucida (MBF Bioscience) routines were used, as described previously[78] to quantify the density of LCs revealed by EGFP and GFP immunolabeling in the epidermis and the density of cutaneous innervation revealed by PGP immunolabeling. Detailed images and descriptions of the mapping and quantification procedures are shown in prior publications.[70,71,78]All quantification was expressed as the number of LCs and neural profiles per mm of epidermal length averaged from 3 sections per specimen. Langerhans cells were further quantified according to their relative deep to superficial locations in the epidermis. As described previously, innervation density was quantified based on 4 criteria: (1) density of upper dermal nerve fibers that are small nerves and axons in the upper dermis that are the source of sensory endings in the upper dermis and epidermis; (2) density of subepidermal nerve fibers, which are terminal branches of small nerves in contact with the epidermal basement membrane; (3) density of entry points, where sensory axons penetrate the basement membrane to enter the epidermis; and (4) density of IENFs, which are the sensory axon endings in the epidermis, regardless of whether their entry was present in the plane of sectioning.

2.9. Statistical analyses

Data were analyzed using SPSS 27 (SPSS Inc, Chicago, IL). The Shapiro–Wilk test was performed to determine whether data were normally distributed and appropriate for applying parametric statistics. The Levene test was used to assess homogeneity of variance. In vitro data comparing mRNA expression levels of GFP

and CB_2 and impact of drug treatments on mRNA levels of various chemokines or cytokines were analyzed using unpaired sample *t* tests (Welch correction applied when appropriate). In vivo behavioral data involving 2 variables (eg, treatment and time) across multiple groups were analyzed by repeated-measures 2-way analysis of variance (ie, when behavioral measures were evaluated in the same animals at different times) followed by the Bonferroni post hoc test in each case. Planned comparisons between 2 groups were performed using unpaired-sample or paired-sample t tests, as appropriate for between-group or within-group comparisons, respectively. $P < 0.05$ was considered statistically significant. Figures were generated using GraphPad Prism version 7.03 (La Jolla, CA).

3. Results

3.1. Comparison of mRNA levels of green fluorescent protein and CB_2 in the spleen, lumbar spinal cord, and paw skin derived from wild type and CB_2^{EGFP} mice

In this study, we used a transgenic mouse line (CB_2^{EGFP}) which couples the EGFP reporter gene to *cnr2* gene transcription[55] as a surrogate means to document the expression and distribution of CB_2. CB_2 mRNA expression levels did not differ between WT and CB_2^{EGFP} mice in the spleen ($P = 0.354$) by qPCR, indicating that insertion of GFP did not alter the basal expression level of CB_2 mRNA in the spleen (**Fig. 1A**). Similarly, CB_2 mRNA was expressed at comparable levels in the lumbar spinal cord ($P = 0.16$, **Fig. 1B**) and paw skin ($P = 0.418$, **Fig. 1C**) of WT and CB_2^{EGFP} mice. By contrast, GFP mRNA was only present in CB_2^{EGFP} mice relative to WT mice in the spleen ($P = 0.0001$, **Fig. 1D**), lumbar spinal cord ($P = 0.0001$, **Fig. 1E**), and paw skin ($P = 0.004$, **Fig. 1F**).

Next, we compared CB_2 and GFP mRNA levels in the spleen, lumbar spinal cord, and paw skin derived from CB_2^{EGFP} mice treated with either paclitaxel or its cremophor-based vehicle as indicated in Methods. In mice euthanized during the maintenance phase of paclitaxel-induced CIPN, when mechanical and cold allodynia were established and stable, CB_2 mRNA expression levels did not differ between paclitaxel and cremophor vehicle–treated groups in the spleen ($P = 0.566$, **Fig. 2A**), spinal cord ($P = 0.934$, **Fig. 2B**), or paw skin ($P = 0.21$, **Fig. 2C**). Similarly, no differences were observed in GFP mRNA expression levels between paclitaxel and cremophor vehicle–treated groups in the spleen ($P = 0.48$, **Fig. 2D**), lumbar spinal cord ($P = 0.315$, **Fig. 2E**), or paw skin ($P = 0.398$, **Fig. 2F**) during the maintenance phase of CIPN.

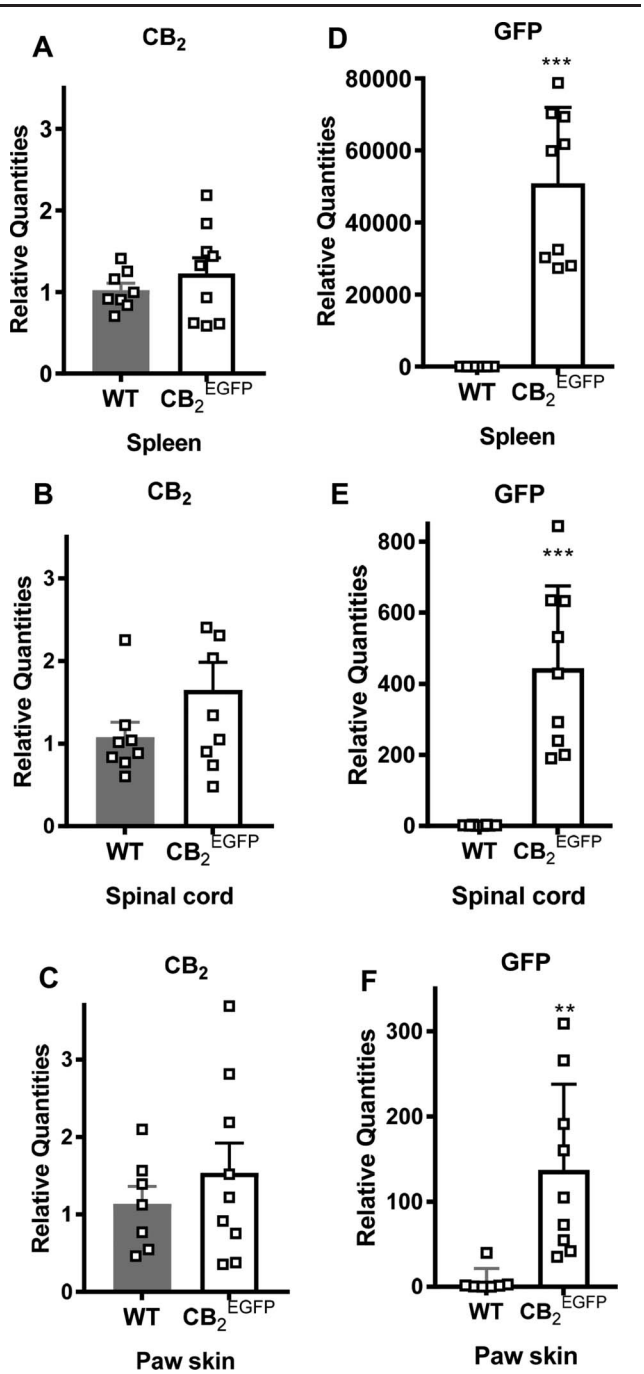

Figure 1. Comparison of CB_2 and GFP mRNA in the spleen, lumbar spinal cord, and paw skin of wild type mice and CB_2^{EGFP} mice. CB_2 mRNA expression levels were comparable in WT and CB_2^{EGFP} mice in either (A) spleen, (B) lumbar spinal cord, or (C) paw skin (n = 8-9/group, mixed sex). Comparison of GFP mRNA expression levels in WT mice and CB_2^{EGFP} mice in (D) spleen, (E) lumbar spinal cord, and (F) paw skin (n = 7-9/group, mixed sex). $^{**}P < 0.01$, $^{***}P < 0.001$, unpaired sample *t* test (Welch correction applied when appropriate). EGFP, enhanced green fluorescent protein; GFP, green fluorescent protein.

3.2. Paclitaxel-induced allodynia developed in CB_2^{EGFP} reporter mice

To determine whether GFP altered paclitaxel-induced allodynia, we compared the development of paclitaxel-induced neuropathic nociception in male and female CB_2^{EGFP} mice. Because no sex difference in responding to mechanical or cold stimulation was observed in animals treated with cremophor-based vehicle (data not shown), we combined equivalent number of male and female mice to generate a single mixed sex cremophor vehicle-treated group (n = 6) to use in subsequent statistical analyses. Both paclitaxel-treated male and female mice were compared with this same mixed sex cremophor vehicle–treated control group. Before treatment with paclitaxel or vehicle (ie, day 0), there were no differences between groups in paw withdrawal thresholds to mechanical stimulation ($P \geq 0.350$, **Fig. 3A**) or duration of responsiveness to cold stimulation ($P \geq 0.141$, **Fig. 3B**). Paclitaxel decreased paw withdrawal thresholds, mechanical responsiveness differed across test days, and the effects of paclitaxel were time dependent (group: $F_{2, 15} = 160.175$, $P < 0.0001$; time: $F_{4, 60} = 132.002$, $P < 0.0001$; and interaction: $F_{8, 60} = 25.32$ $P < 0.0001$, **Fig. 3A**). Paclitaxel also increased the duration of responses to cold, cold responsiveness differed across test days, and the effects of paclitaxel on cold

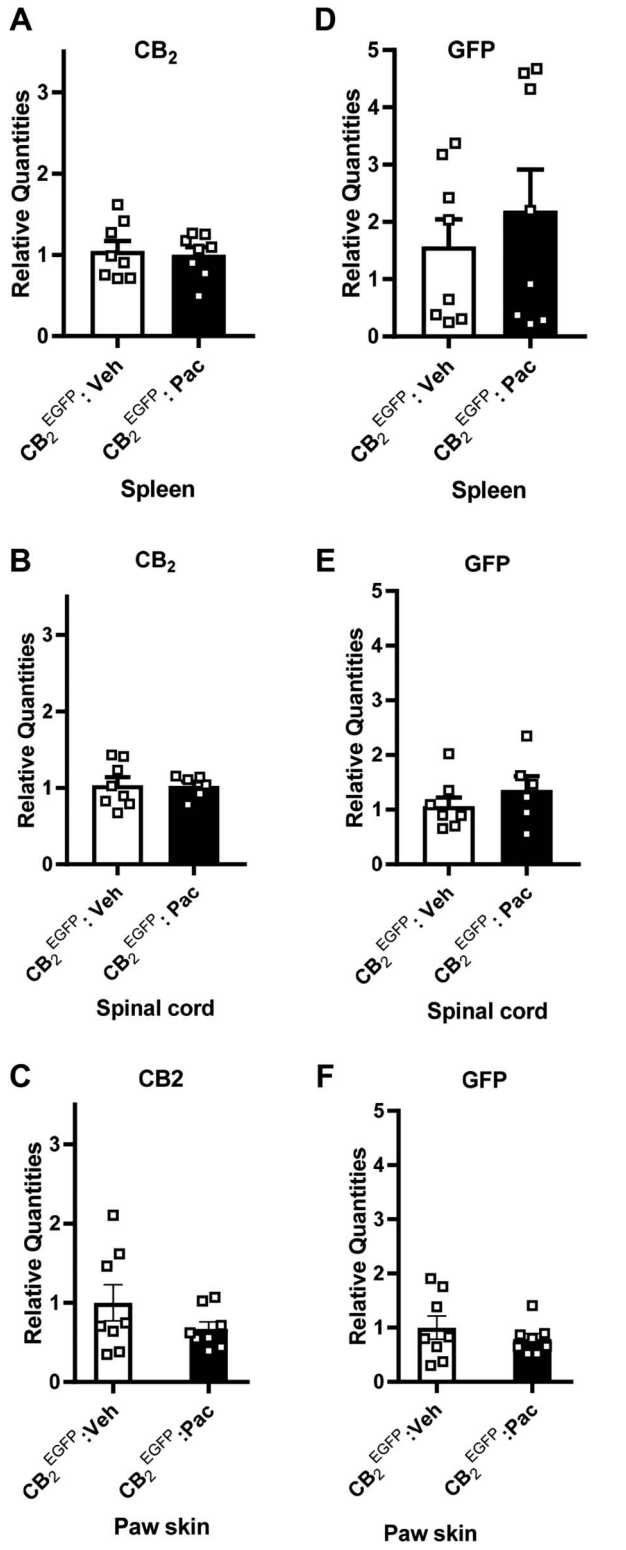

Figure 2. Comparison of CB_2 and GFP mRNA in the spleen, lumbar spinal cord, and paw skin from CB_2^{EGFP} mice treated with paclitaxel or its vehicle. CB_2 mRNA levels did not differ between CB_2^{EGFP} mice treated with paclitaxel or its vehicle in either (A) spleen, (B) lumbar spinal cord, or (C) paw skin (n = 6-8/group). GFP mRNA did not differ between CB_2^{EGFP} mice treated with paclitaxel or its vehicle in either (D) spleen, (E) lumbar spinal cord, or (F) paw skin (n = 6-8/group, mixed sex). Unpaired sample *t* test (Welch correction applied when appropriate). EGFP, enhanced green fluorescent protein; GFP, green fluorescent protein.

responsiveness were also time dependent (group: $F_{2, 15} = 18.885$, $P < 0.0001$; time: $F_{4, 60} = 31.506$, $P < 0.0001$; and interaction: $F_{8, 60} = 6.89$, $P < 0.0001$, **Fig. 3B**) in CB_2^{EGFP} mice. Mechanical (**Fig. 3A**) and cold (**Fig. 3B**) allodynia started to develop on day 4 (mechanical $P < 0.0001$; cold $P \leq 0.006$) after initiation of paclitaxel dosing and was maintained with high stability in paclitaxel-treated CB_2^{EGFP} mice relative to cremophor-vehicle treatment from day 7 onward (mechanical $P < 0.0001$ and cold $P \leq 0.002$ for each test time point) for the duration of testing. No sex differences in response to mechanical ($P \geq 0.543$) or cold ($P = 1$) stimulation were observed at any time point during either the development or maintenance of paclitaxel-induced neuropathic nociception. Meanwhile, we also found that WT mice[52] and CB_2^{EGFP} mice used in this study showed statistically comparable development and maintenance of paclitaxel-induced neuropathic nociception throughout the observation interval (data not shown).

3.3. CB_2 agonists dose dependently suppressed paclitaxel-induced neuropathic nociception in CB_2^{EGFP} mice

LY2828360, a CNS-penetrant CB_2 agonist, was administered by i.p. injection in paclitaxel-treated CB_2^{EGFP} male and female mice exhibiting established CIPN. Before agonist injections, paclitaxel reduced mechanical thresholds ($P < 0.0001$, **Fig. 3C**) and increased the duration of responsiveness to cold stimulation ($P < 0.0001$, **Fig. 3D**) relative to baseline (BL) levels. LY2828360 dose dependently suppressed paclitaxel-induced mechanical (treatment: $F_{1, 19} = 201.9$, $P < 0.0001$; dose: $F_{6, 114} = 13.45$, $P < 0.0001$; and interaction: $F_{6, 114} = 24.64$, $P < 0.0001$, **Fig. 3C**) and cold (treatment: $F_{1, 19} = 16.84$, $P = 0.001$; dose: $F_{6, 114} = 18.09$, $P < 0.0001$; and interaction: $F_{6, 114} = 17.08$, $P < 0.0001$, **Fig. 3D**) allodynia. Mechanical paw withdrawal thresholds were elevated at doses of 0.3 mg/kg or higher relative to vehicle-treated animals ($P < 0.001$, **Fig. 3C**). Similarly, the duration of cold responsiveness was lowered at doses of 1 mg/kg or higher tested doses relative to vehicle-treated animals ($P < 0.01$, **Fig. 3D**).

Next, we tested another CB_2 agonist, AM1710, which exhibits lower brain penetration compared with other CB_2 ligands screened after intravenous administration in rats.[75] AM1710, administered systemically, suppressed paclitaxel-induced mechanical (treatment: $F_{1, 19} = 74.52$, $P < 0.0001$; dose: $F_{4, 76} = 16.43$, $P < 0.0001$; and interaction: $F_{4, 76} = 33.59$, $P < 0.0001$, **Fig. 3E**) and cold (treatment: $F_{1, 19} = 45.03$, $P < 0.0001$; dose: $F_{4, 76} = 21.79$, $P < 0.0001$; and interaction: $F_{4, 76} = 32.561$, $P < 0.0001$, **Fig. 3F**) allodynia. AM1710 suppressed paclitaxel-induced mechanical ($P < 0.0001$, **Fig. 3E**) and cold ($P < 0.0001$, **Fig. 3F**) responsiveness at doses of 3 mg/kg i.p. or higher.

3.4. Antiallodynia effects of AM1710 were blocked by the CB_2 antagonist SR144528

To further investigate peripheral sites of AM1710-induced antiallodynia action and whether tolerance is present after chronic injection, SR144528 (2.1 mg/kg per day, × 8 days), a CB_2 antagonist that exhibits limited CNS penetration in mouse[11] was administered i.p. to paclitaxel-treated CB_2^{EGFP} male and female mice either alone or in combination with AM1710 for 8 days (5 mg/kg per day i.p. × 8 days). Systemic drug treatments altered paclitaxel-induced hypersensitivity to mechanical and cold

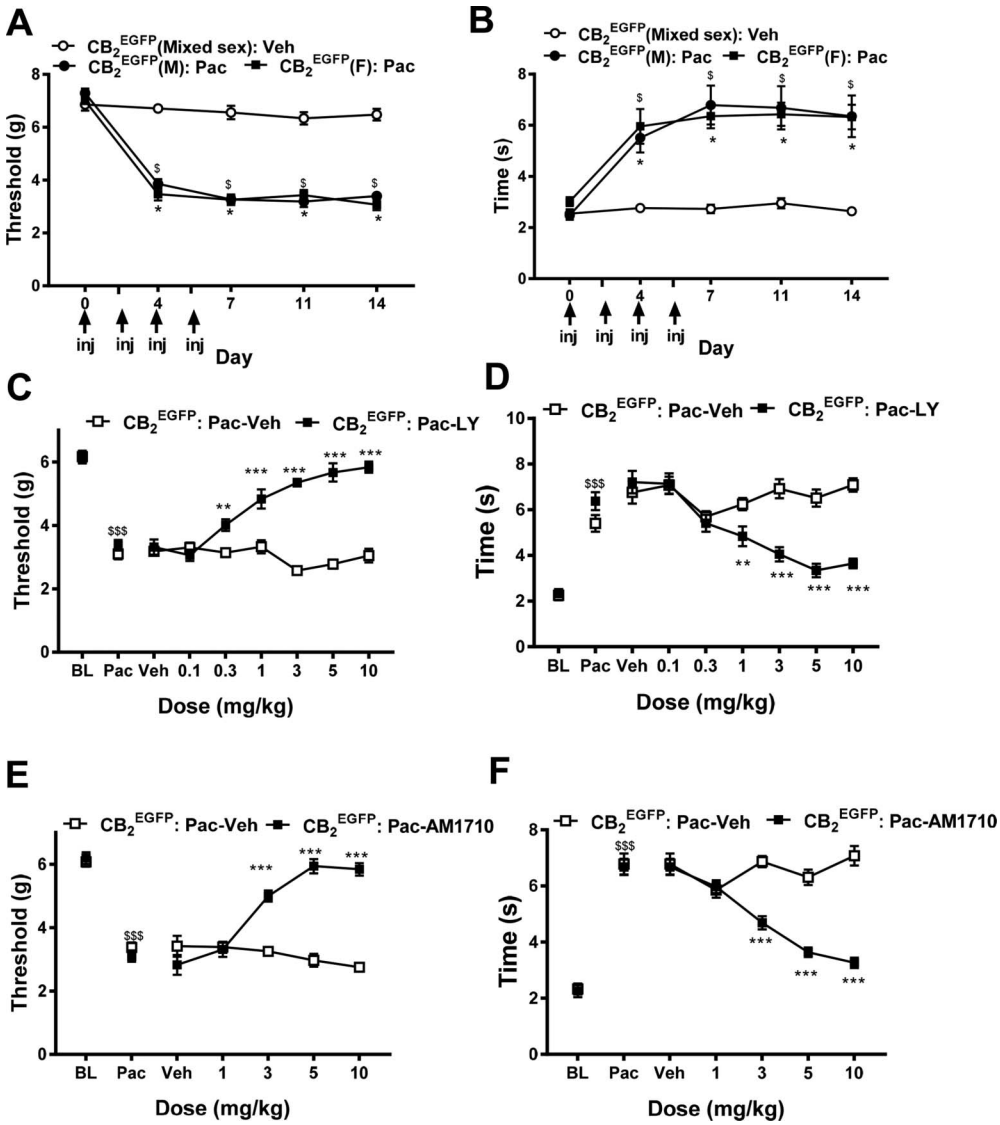

Figure 3. Paclitaxel produces hypersensitivity to mechanical (A) and cold (B) stimulation in CB_2^{EGFP} mice (n = 6/group). Dose response of (C and D) LY2828360 (0.1-10 mg/kg i.p.) and (E and F) AM1710 (1-10 mg/kg i.p.) in suppressing the maintenance of paclitaxel-induced neuropathic nociception in CB_2^{EGFP} mice (n = 10-11/group, mixed sex), as measured by paw withdrawal thresholds to mechanical stimulation (C and E) and duration of responding to cold stimulation (D and F). Data are expressed as mean ± SEM. (A–B) * $P < 0.05$ (male), $ $P < 0.05$ (female) vs vehicle-treated control (mixed sex), 2-way repeated measures ANOVA followed by the Bonferroni post hoc test. (C–F) ** $P < 0.01$; *** $P < 0.001$ vs corresponding vehicle, repeated measures 2-way ANOVA followed by the Bonferroni post hoc test. $$$ $P < 0.001$ vs corresponding BL, paired sample *t* test. ANOVA, analysis of variance; BL, baseline; EGFP, enhanced green fluorescent protein.

stimulation, behavioral hypersensitivities changed across time, and the interactions were significant for each modality (mechanical: treatment: $F_{3, 25} = 35.675$, $P < 0.0001$; time: $F_{4, 100} = 135.29$, $P < 0.0001$; and interaction: $F_{12, 100} = 9.885$, $P < 0.0001$, **Fig. 4A**; cold: treatment: $F_{3, 25} = 25.139$, $P < 0.0001$; time: $F_{4, 100} = 87.9$, $P < 0.0001$; and interaction: $F_{12, 100} = 5.748$, $P < 0.0001$, **Fig. 4B**). AM1710 (5 mg/kg/day i.p x 8 days) alone suppressed paclitaxel-induced mechanical and cold allodynia compared with all other groups (mechanical $P < 0.0001$, cold $P \leq 0.007$, **Figs. 4A and B**) at every time point tested. SR144528 (2.1 mg/kg per day i.p. x 8 days) alone did not alter mechanical or cold responsiveness relative to vehicle treatment in CB_2^{EGFP} reporter mice at any observation interval (mechanical $P > 0.9999$, cold $P \geq 0.671$, **Figs. 4A and B**). The CB_2 antagonist SR144528 blocked the antiallodynic effects of AM1710; the combination of SR144528 (2.1 mg/kg per day × 8 days) with AM1710 (5 mg/kg per day × 8 days) prevented antiallodynia relative to postpaclitaxel baseline (Pac) responding on all injection days (mechanical $P \geq 0.491$ and cold $P \geq 0.727$). Furthermore, when AM1710 was combined with SR144528, antiallodynia responses were absent relative to mice treated with AM1710 alone (mechanical $P < 0.0001$, cold $P \leq 0.007$, **Figs. 4A and B**) throughout the entire 8 day testing interval, consistent with a peripheral antinociceptive mechanism.

3.5. Intraplantar administration of AM1710 suppressed paclitaxel-induced allodynia in CB_2^{EGFP} reporter mice but not in CB_2 knock out mice

In paclitaxel-treated CB_2^{EGFP} reporter mice, AM1710 (30 μg, i.pl.) suppressed mechanical allodynia in the ipsilateral (injected) paw, paw withdrawal thresholds changed across time, and the interaction between time and treatment was significant (treatment: $F_{1, 10} = 12.687$, $P = 0.005$; time: $F_{3, 30} = 10.11$ $P <$

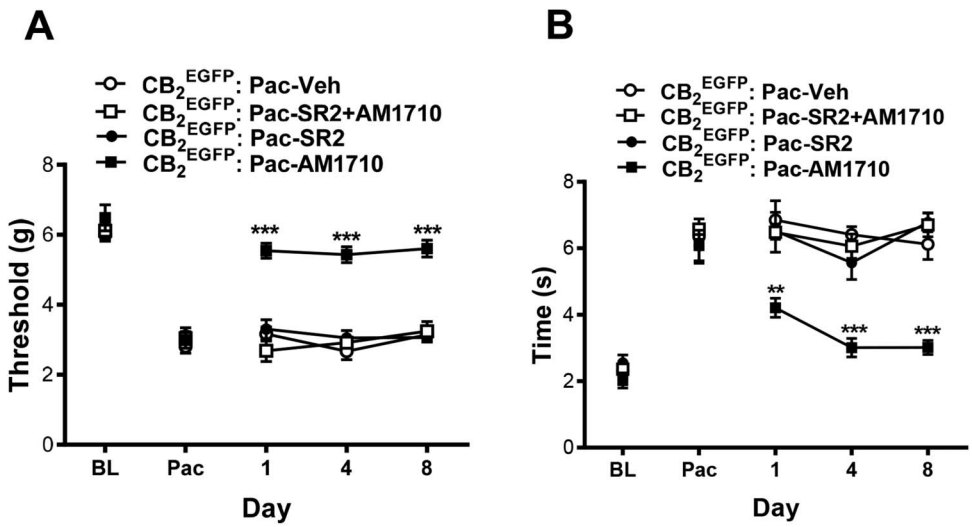

Figure 4. Antiallodynic effects of AM1710 in CB_2^{EGFP} mice were blocked by a peripherally restricted CB_2 antagonist during the maintenance of paclitaxel-induced neuropathic nociception. AM1710 (5 mg/kg per day i.p. × 8 days) suppressed paclitaxel-induced (A) mechanical and (B) cold allodynia in a manner that was blocked by SR144528 (2.1 mg/kg per day i.p. × 8 days). Data are expressed as mean ± SEM. (n = 7-8/group; mixed sex). $^{**}P < 0.01$, $^{***}P < 0.001$ vs corresponding control group, repeated measures 2-way ANOVA followed by the Bonferroni post hoc test. BL, baseline before paclitaxel; Pac, baseline after paclitaxel. ANOVA, analysis of variance; BL, baseline; EGFP, enhanced green fluorescent protein.

0.0001; and interaction: $F_{3, 30} = 3.41$, $P = 0.03$, **Fig. 5A**). Local injection of AM1710 increased mechanical paw withdrawal thresholds at both 30 minutes and 1.5 hours postinjection relative to vehicle-treated animals, respectively (30 minutes: $P = 0.026$, 1.5 hours: $P = 0.02$, **Fig. 5A**). Similarly, unilateral intraplantar injection of AM1710 (30 μg, i.pl.) altered paclitaxel-induced cold hypersensitivity in the paw ipsilateral to the injection, but the interaction between time and treatment was not significant (treatment: $F_{1, 10} = 7.216$, $P = 0.023$; time: $F_{3, 30} = 3.99$, $P = 0.017$; interaction: $F_{3, 30} = 2.16$, $P = 0.113$, **Fig. 5B**). AM1710 reduced cold responsiveness at both 30 minutes ($P = 0.017$) and 1.5 hours after drug injection ($P = 0.011$, **Fig. 5B**). Antiallodynic efficacy of AM1710 was no longer apparent by 2.5 hours after injection (mechanical: $P = 0.812$, cold: $P = 0.582$, **Fig. 5A, B**). Local injection of AM1710 (30 μg, i.pl.) did not alter mechanical or cold responsiveness in the paw contralateral to injection (data not shown), indicating that AM1710 (30 μg, i.pl.) produced antiallodynia that was mediated locally in the paw. Furthermore, local injection of AM1710 (30 μg, i.pl.) did not alter responsiveness to either mechanical or cold stimulation relative to intraplantar injection of vehicle in CB_2^{EGFP} mice receiving cremophor vehicle in lieu of paclitaxel (mechanical $P > 0.999$, cold $P \geq 0.6779$, **Figs. 5C and D**). Thus, AM1710 selectively suppressed neuropathic nociception through a local site of action without producing antinociception.

Next, we verified whether antiallodynic efficacy of local i.pl. injection of AM1710 was absent in CB_2KO mice. Before paclitaxel treatment, there were no differences between CB_2^{EGFP} mice and CB_2KO mice in paw withdrawal thresholds to mechanical stimulation (BL: $P = 0.705$, **Fig. 5E**) or duration of responses to cold stimulation (BL: $P = 0.101$, **Fig. 5F**). Paclitaxel altered mechanical paw withdrawal thresholds and duration of cold responses in both CB_2^{EGFP} mice (mechanical: $P < 0.0001$; cold: $P = 0.00132$) and CB_2KO mice (mechanical: $P = 0.000256$; cold: $P = 0.00663$, **Fig. 5 E** and **F**). AM1710 (30 μg, i.pl.) elevated mechanical paw withdrawal thresholds and reduced cold responses in CB_2^{EGFP} mice (mechanical $P < 0.0001$, cold $P = 0.001$) but not in CB_2KO mice (mechanical $P = 0.79$, cold $P = 1$) at 30 minutes postinjection relative to their corresponding postpaclitaxel levels (Pac). CB_2^{EGFP} mice receiving AM1710 (30 μg i.pl.) exhibited higher mechanical paw withdrawal thresholds and shorter duration of cold responses compared with CB_2KO mice at 30 minutes after injection (mechanical $P = 0.007$ and cold $P = 0.014$). Antiallodynic efficacy of AM1710 (30 μg i.pl.) was no longer detected in CB_2^{EGFP} mice, relative to the corresponding postpaclitaxel levels, at 2.5 hours after injection (mechanical $P = 1$ and cold $P = 0.239$). Intraplantar AM1710 did not alter mechanical withdrawal thresholds or duration of cold responses in CB_2KO mice, compared with their corresponding postpaclitaxel levels, at any timepoint throughout the testing interval (mechanical $P \geq 0.790$, cold $P = 1$). Thus, the antiallodynic efficacy of intraplantar AM1710 was mediated by a peripheral CB_2 mechanism.

3.6. Impact of intraplantar AM1710 on mRNA expression levels of cytokines and chemokines in the lumbar spinal cord

To further explore the mechanism of peripheral CB_2-mediated antihyperalgesia, we examined the impact of intraplantar AM1710 on mRNA expression levels of cytokines and chemokines during the maintenance of paclitaxel-induced neuropathy in CB_2^{EGFP} male and female mice. The mRNA level of anti-inflammatory cytokine IL-10 was increased in the lumbar spinal cord after AM1710 (30 μg, i.pl.) relative to vehicle injection ($P = 0.019$, **Fig. 6**). An increase in TNF-α ($P = 0.032$, **Fig. 6**) and MCP-1 ($P = 0.012$, **Fig. 6**) mRNA expression levels were also observed in the same samples. By contrast, no differences in mRNA expression levels of IL-1β ($P = 0.059$) or IL-6 ($P = 0.181$) were detected.

3.7. Paclitaxel altered CB_2 promoter–driven green fluorescent protein expression and CB_2 coimmunolabeling on hind paw epidermal keratinocytes

As a surrogate for CB_2 expression, we surveyed anti-GFP immunolabeling in CB_2^{EGFP} reporter mice in a variety of tissues

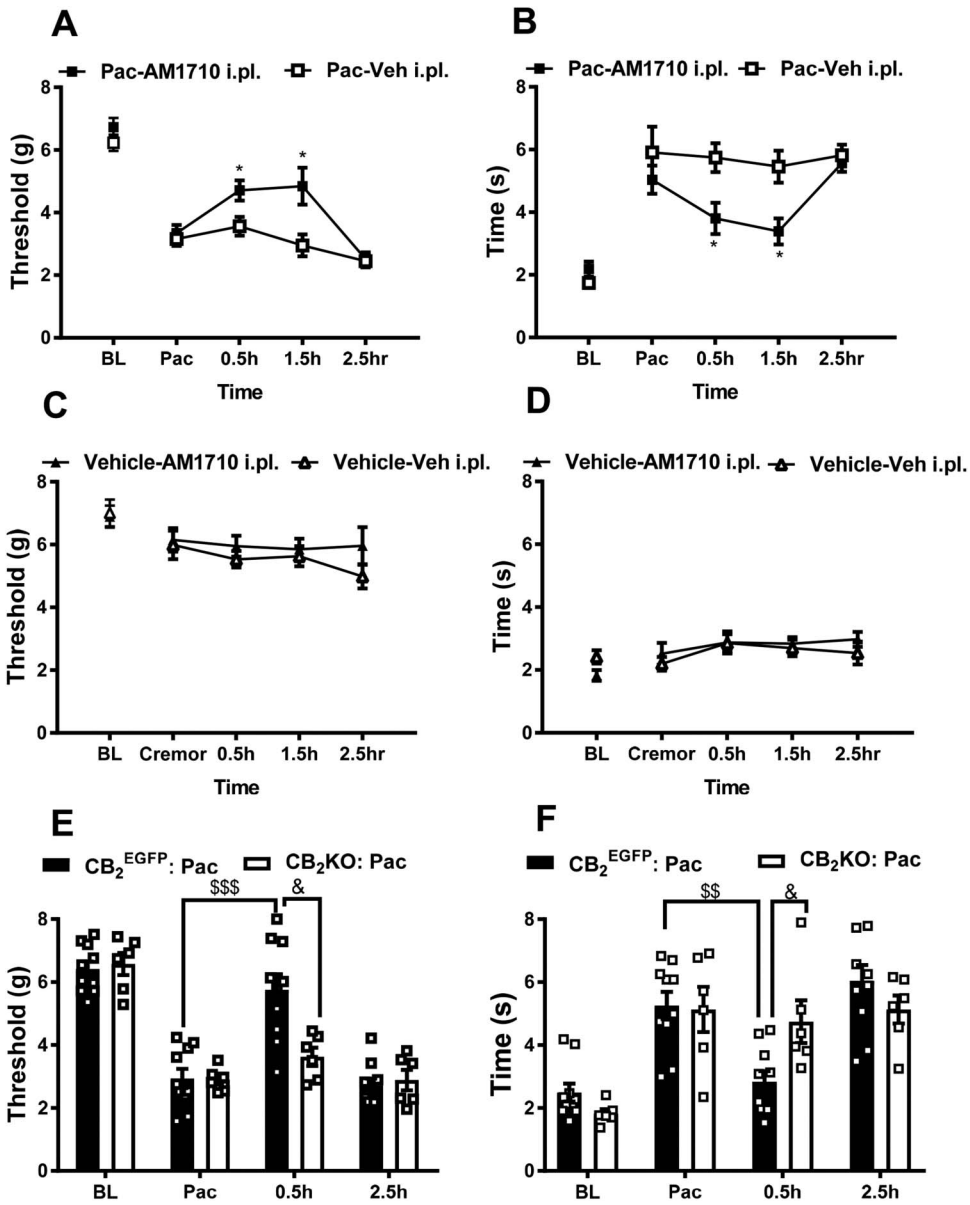

Figure 5. Intraplantar administration of AM1710 selectively suppressed paclitaxel-induced neuropathic nociception in CB_2^{EGFP} male mice but not in CB_2KO mice. In paclitaxel-treated CB_2^{EGFP} mice, local injection of AM1710 (30 μg i.pl.) in the paw suppressed behavioral hypersensitivity to (A) mechanical and (B) cold stimulation. In cremophor vehicle–treated mice, intraplantar AM1710 (30 μg i.pl.) did not alter responsiveness to (C) mechanical and (D) cold stimulation relative to vehicle (i.pl.) injection. Local injection of AM1710 (30 μg i.pl.) in the paw suppressed behavioral hypersensitivity to (E) mechanical and (F) cold stimulation in paclitaxel-treated CB_2^{EGFP} but not CB_2KO mice. Paw withdrawal thresholds in contralateral (noninjected paw) did not differ between groups in any study (data not shown). Data are expressed as mean ± SEM. (A and B) n = 6 male mice/group; C and D: n = 6-7 male mice/group; E and F: n = 6 male mice in CB_2KO group and n = 10 male mice in CB_2^{EGFP} group). *$P < 0.05$ vs vehicle (i.pl.) control in lieu of AM1710, & $P < 0.05$ vs.CB_2KO animals, repeated measure 2-way ANOVA followed by the Bonferroni post hoc test; \$\$<0.01 vs Pac in CB_2^{EGFP} mice, \$\$\$ $P < 0.001$ vs Pac in CB_2^{EGFP} mice, paired sample 2-tailed *t* test; BL, baseline before paclitaxel; Pac, baseline after paclitaxel. ANOVA, analysis of variance; BL, baseline; EGFP, enhanced green fluorescent protein.

including the spleen, lumbar spinal cord, and brain. An anti-GFP signal was not detected in the spleen of wild type mice (**Fig. 7A**), whereas a robust signal was detected in the spleen of both vehicle-treated and paclitaxel-treated CB_2^{EGFP} mice (**Figs. 7B and C**). The anti-GFP signal was also absent in the lumbar spinal cord derived from wild type mice as expected (**Fig. 8A**). Moreover, we did not observe anti-GFP immunolabeling in the lumbar spinal cord of either paclitaxel-treated or vehicle-treated CB_2^{EGFP} mice (**Figs. 8B and C**). Similarly, we did not detect anti-GFP immunolabeling in the brain of wild type mice (**Fig. 9A**) or in the brain of CB_2^{EGFP} mice treated with either paclitaxel or vehicle (**Figs. 9B and C**).

Paclitaxel treatment has long been known to have adverse effects on many nonmalignant cell types having high turnover rates such as epidermal keratinocytes.[82] To evaluate the impact of paclitaxel treatment on CB_2^{EGFP} mouse keratinocytes, the glabrous hind paw skin was assessed using combinations of endogenous EGFP fluorescence with immunofluorescence for GFP and CB_2 protein. A good alignment between the distribution and intensity levels of EGFP fluorescence and immunolabeling for GFP protein and CB_2 protein was observed, especially for the vehicle-treated specimen (**Fig. 10A-C**). In the vehicle-treated specimen, all 3 fluorescent labels were fairly uniformly expressed across the keratinocytes of stratum basalis (SB), stratum

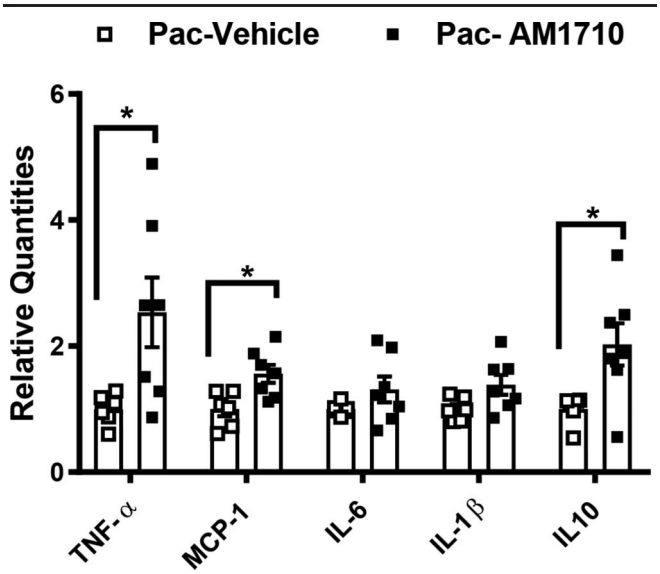

Figure 6. Impact of paclitaxel and the CB_2 agonist AM1710 on cytokine and chemokine mRNA expression levels in the lumbar spinal cord from CB_2^{EGFP} mice. Acute intraplantar injection of AM1710 (30 μg i.pl.) increased the spinal mRNA levels of anti-inflammatory cytokine IL-10 and proinflammatory cytokine TNF-α and MCP-1. Data are expressed as mean ± SEM. (n = 6-7 mixed sex/group). * $P < 0.05$ vs vehicle in lieu of AM1710, unpaired sample 2 tailed *t* test. EGFP, enhanced green fluorescent protein; IL-10, interleukin-10; MCP-1, monocyte chemoattractant protein-1; TNF-tumor necrosis factor alpha.

spinosum (SS), and stratum granulosum (SG) (between the larger broad arrowheads in **Figs. 10A–C** and Fig. S1A-C, available at http://links.lww.com/PAIN/B516). Slightly higher expressions of all 3 fluorescent labels were evident among discontinuous locations across SB in the vehicle-treated specimen (broken line contours, **Figs. 10A–C**). Also, there were discontinuous thin strata of slightly higher GFP and CB_2 immunolabeling at the transition from SS to SG (between the smaller broad arrows in **Figs. 10B and C**). Fluorescence expression was low for all 3 markers among the live enucleated, lipid-enriched keratinocytes of stratum lucidum. Little expression occurred among the thick dead layer of keratinocyte of stratum corneum (SC), of which a loose outer layer often separated from the surface of SC (asterisks). As shown in **Figure 10C**, EGFP and CB_2R_{nt}-Cy3 was detected among Merkel cells in SB (yellow oval outline). Some dendritic cells (curved arrows) in the upper dermis and LCs (narrow arrows) in the epidermis expressed EGFP and GFP-Cy3 but did not label for CB_2R_{nt}.

The specimens derived from paclitaxel-treated CB_2^{EGFP} mice exhibited considerable differences from vehicle among the 3 fluorescent patterns (**Fig.10D-F**; Fig. S1D-F, available at http://links.lww.com/PAIN/B516). In **Figure 10D**, left image, combined GFP-Alex488 and EGFP imaging reveals a high level of green signal across all keratinocytes in SB, SS, and SG (broad solid arrows). However, as seen in the middle and right images, EGFP digital captures taken before GFP-Alexa488 processing revealed a high level of EGFP in SG and the upper half of SS (between broad solid arrows), whereas EGFP was expressed at much lower levels in SB and the lower half of SS (open broad arrows) where there was a high level of immunolabeling for GFP-Alexa488. This pattern is confirmed in **Figure 10E** where EGFP fluorescence is high in SG and upper SS, but GFP-Cy3 is relatively low (between broad yellow and green arrows), whereas EGFP is low in SB and lower SS, but GFP-Cy3 is high (between broad yellow and red arrows). As shown in **Figure 10F**, the patterns of EGFP and CB_2R_{nt}-Cy3 are identical to those of EGFP and GFP-Cy3. To exclude the possible nonspecificity of antibodies used in this study, we also stained the hind paw tissue from wildtype controls with only the secondary antibodies used in this study. The images in **Figure 10G and H** were stained with donkey anti-rabbit Cy3 and donkey anti-rabbit Alexa488, respectively. The image in **Figure 10I** was stained with anti-GFP primary antibody and secondary antibody. Our results thus confirm the specificities of the antibodies in our study.

Furthermore, numerous exceptionally branched dendritic cells localize to the upper dermis (curved arrows) and LCs (narrow straight arrows) to the epidermis where they are concentrated at the mid-SS level. Both the dendritic and LCs are labeled for EGFP and GFP but not N-terminal domain of CB_2 (CB_2R_{nt}, **Fig. 10C, F**; S1, available at http://links.lww.com/PAIN/B516). However, a retrospective assessment of the normal rat skin (unpublished pilot study) revealed that dendritic cells and LCs labeled with a rabbit polyclonal antibody raised against a rat C-terminal sequence but not the N-terminal sequence (antibodies created by K. Mackie, no longer available; Fig. S2A, B, available at http://links.lww.com/PAIN/B516). Although these immunolabeling results suggest there may be a conformational variant of CB_2 expressed by LCs, quantification based on the EGFP and GFP protein expression revealed that LCs were significantly increased in the epidermis of the paclitaxel-treated specimen where they were concentrated at the midepidermal transition from SS to SG (**Figs. 11A and B**).

Protein gene product 9.5 immunolabeling revealed that, following paclitaxel dosing, previously known types of innervation remain (**Fig. 12**). This included sensory endings in the epidermis (IENF) that are supplied by putative C-fiber nociceptors and that may have actually increased compared with that observed in the vehicle-treated specimen (**Fig. 13**). Our previous use of the identical quantification procedure in unpublished similar mouse and rat CIPN studies on behalf of MD Anderson and 2 pharmaceutical companies revealed that significant decreases and increases as well as no significant differences in epidermal innervation densities can occur depending on slight differences in the treatment and posttreatment survival protocols. No definitive EGFP, GFP, or CB_2 expression was detected among morphological varieties of sensory endings from different types of myelinated and unmyelinated DRG neurons. However, CB_2 immunolabeling was detected on some larger caliber axons located in the small nerves of the dermis (curved arrows, **Fig. 12**). A robust expression was also detected among the Merkel cell accessories to Merkel endings in SB (oval contours in **Figs. 10C** and **12B**).

4. Discussion

We used a transgenic (CB_2^{EGFP}) mouse line to document CB_2 expression and distribution in a CIPN model and circumvent problems associated with nonspecific CB_2 antibody staining. GFP immunolabeling, a surrogate marker of CB_2, showed that CB_2 was dynamically regulated under conditions of paclitaxel-induced neuropathy at peripheral sites; labeling included keratinocytes, Merkel cells, and LCs in paw tissue. Signals were below the threshold for detection in CNS. This expression pattern confirms results of functional and mechanistic data presented in this report.

We postulate that CB_2 agonists suppress paclitaxel-induced allodynia through a peripheral mechanism. Several lines of evidence support this hypothesis. First, CB_2 agonists that differ in their ability to penetrate the CNS were equally efficacious in suppressing paclitaxel-induced allodynia. Second, antiallodynic

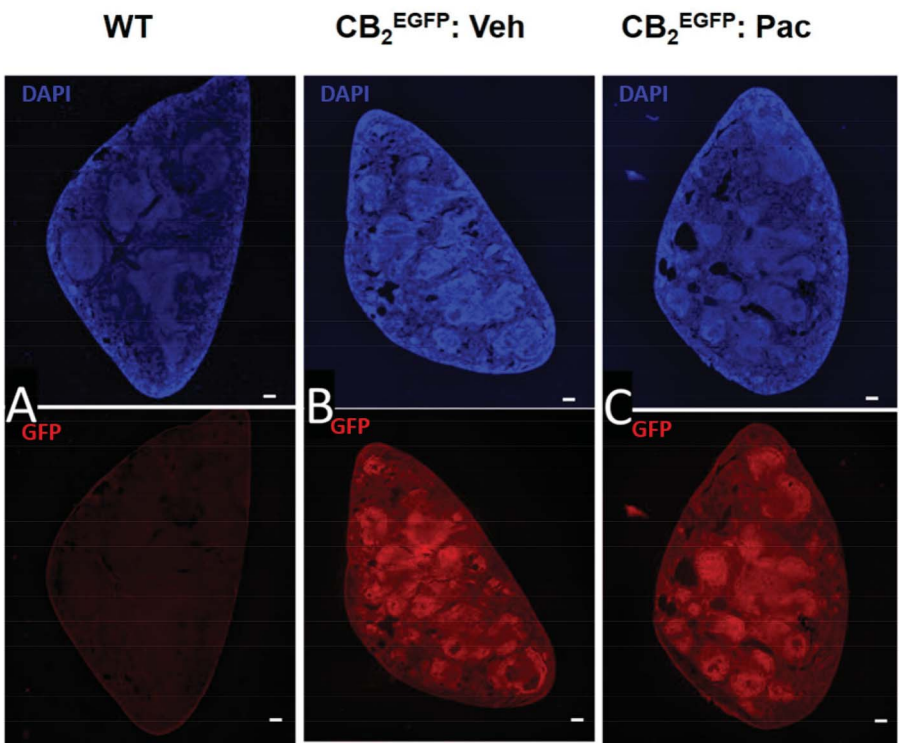

Figure 7. Immunolabeling for GFP in the spleen from untreated wild type mice and CB_2^{EGFP} mice treated with either paclitaxel or its cremophor-based vehicle. Paclitaxel (4 mg/kg i.p. administered on day 0, 2, 4, and 6) or vehicle was administered on 4 alternate days and mice were perfused and tissue dissected during the maintenance phase of CIPN (day 16). Photomicrographs of transverse section of the spleen in (A) untreated wild type mouse, (B) cremophor vehicle–treated CB_2^{EGFP} mouse, and (C) paclitaxel-treated CB_2^{EGFP} mouse immunolabeled with anti-GFP revealed by AlexaFluor 594 (red) and stained with DAPI (blue). Scale bar in image = 100 μm. CIPN, chemotherapy-induced peripheral neuropathy; EGFP, enhanced green fluorescent protein; GFP, green fluorescent protein.

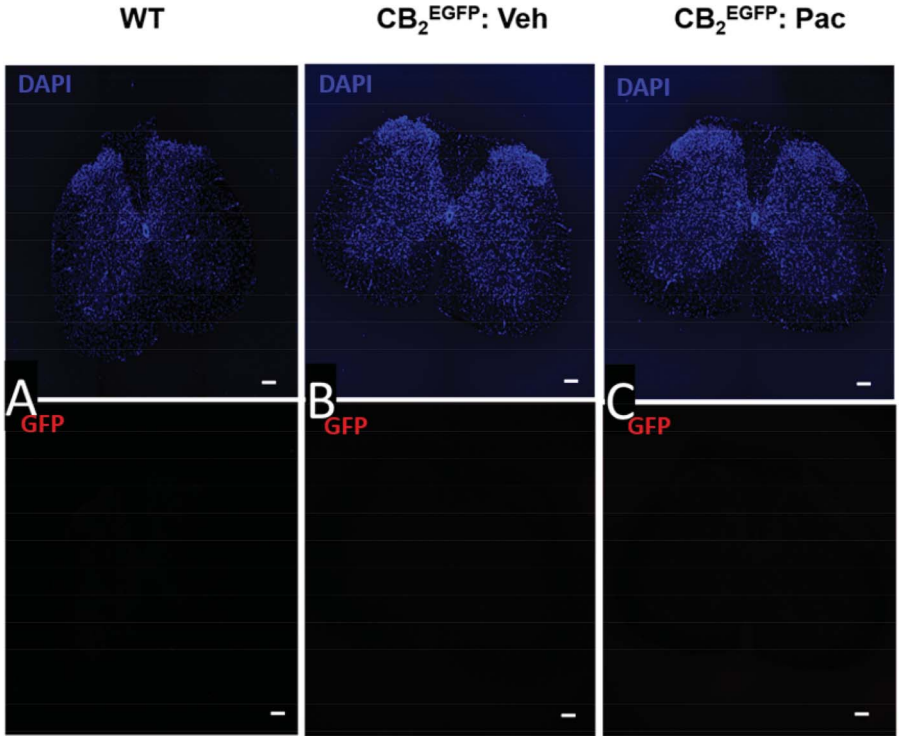

Figure 8. Immunolabeling for GFP was below the threshold for detection in the lumbar spinal cord derived from either naive wild type mice or CB_2^{EGFP} mice treated with either paclitaxel or its cremophor-based vehicle. Paclitaxel (4 mg/kg i.p. administered on day 0, 2, 4, and 6) or vehicle was administered on 4 alternate days and mice were perfused and tissue dissected during the maintenance phase of CIPN (day 16). Photomicrograph of transverse section of mouse lumbar spinal cord section in (A) untreated wild type mouse, (B) vehicle-treated CB_2^{EGFP} mouse, and (C) paclitaxel-treated CB_2^{EGFP} mouse immunolabeled with anti-GFP revealed by AlexaFluor 594 (red) and stained with DAPI (blue). Scale bar in image = 100 μm. CIPN, chemotherapy-induced peripheral neuropathy; EGFP, enhanced green fluorescent protein; GFP, green fluorescent protein.

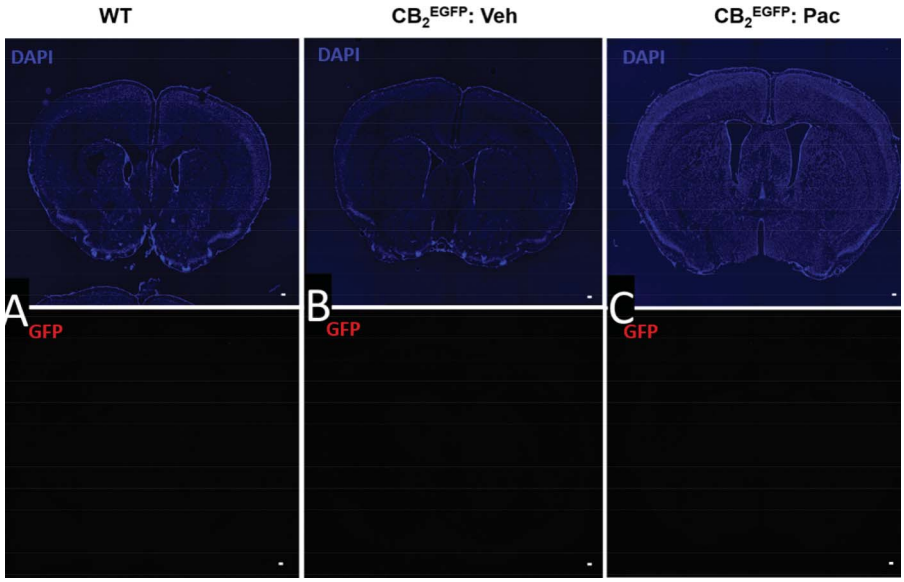

Figure 9. Immunostaining for GFP is below the threshold for detection in coronal brain sections derived from either naive wild type mice or CB_2^{EGFP} mice treated with either paclitaxel or its cremophor-based vehicle. Paclitaxel (4 mg/kg i.p. administered on day 0, 2, 4, and 6) or vehicle was administered on 4 alternate days, and mice were perfused and tissue dissected during the maintenance phase of CIPN (day 16). Photomicrograph of coronal section of the forebrain in (A) untreated wild type mouse, (B) cremophor vehicle–treated CB_2^{EGFP} mouse, and (C) paclitaxel-treated CB_2^{EGFP} mouse was labeled with DAPI (blue) and anti-GFP revealed by AlexaFluor 594 (red). Similar results were observed at all brain levels surveyed throughout the CNS. Scale bar in image = 100 μm. CIPN, chemotherapy-induced peripheral neuropathy; CNS, central nervous system; EGFP, enhanced green fluorescent protein; GPF, green fluorescent protein.

effects of the CB_2 agonist AM1710 were blocked completely by a CB_2 antagonist (SR144528) exhibiting limited CNS penetration.[11] Antiallodynic effects of AM1710 cannot be attributed to CB_1 mechanisms.[21,73,77,94] Third, local hind paw injection of AM1710 reversed paclitaxel-induced allodynia in CB_2^{EGFP} but not CB_2KO mice without producing antinociception in cremophor vehicle–treated mice. Intraplantar AM1710 was unlikely to act systemically (or in the CNS) as unilateral hind paw injection did not alter responsiveness of the hypersensitive paw contralateral to AM1710 injection. This observation is in line with previous work showing that another CB_2 agonist, AM1241, suppressed allodynia in rats after local injection to the ipsilateral (ie, carrageenan or capsaicin-injected) paw.[32,75] Fourth, intraplantar AM1710 injection increased lumbar spinal cord mRNA expression levels of IL-10, an anti-inflammatory cytokine linked to reversal of paclitaxel-induced hypersensitivity.[45] Fifth, GFP immunolabeling was detected in epidermal keratinocytes and LCs in hind paw volar pads of CB_2^{EGFP} mice where it was increased by paclitaxel treatment. Finally, GFP immunolabeling was below the threshold for detection in CNS of paclitaxel-treated mice when allodynia was established and stable. Our studies raise the possibility that epidermal keratinocytes and LCs may be implicated in the antiallodynic effects of CB_2 agonists in CIPN. However, future studies are required to specifically examine the role of the DRG in antiallodynic effects of CB_2 agonists in CIPN.

Neuropathic pain is associated with a proinflammatory state in both human and animal studies.[39] Elevated proinflammatory cytokines are associated with the development of pain, whereas anti-inflammatory cytokines are associated with downregulation of the immune system and neuropathic pain relief.[4,17,21,91] Here, we report that spinal mRNA expression levels of the anti-inflammatory cytokine IL-10 was elevated by intraplantar AM1710 injection, supporting an emerging literature linking IL-10 with the suppression of neuropathic pain using specific IL-10 antibodies and IL-10 KO mice.[45,62] Furthermore, Saroz et al.[79] confirmed CB_2 signaled by G-α-s and induced IL-10 cytokine secretion in human primary leukocytes, reinforcing the potential utility of CB_2 ligands as immunomodulatory therapeutics. Surprisingly, intraplantar administration of AM1710 increased the mRNA level of proinflammatory cytokine TNF-α and chemokine MCP-1 in the lumbar spinal cord in paclitaxel-treated mice which displayed behavioral reversal of allodynia. By contrast, systemic administration of AM1710 suppressed MCP-1 and TNF-α mRNA expression levels in the lumbar spinal cord after either acute or chronic administration.[21] Three reasons may explain this difference. First, intraplantar injection of AM1710 unilaterally in one hind paw might be unable to suppress surges in MCP-1 mRNA expression levels induced by systemic toxic challenge with paclitaxel in the entire lumbar spinal cord. Paclitaxel also produces robust changes in brain resting-state connectivity,[24] as well as proinflammatory cytokine expression levels in DRG.[15] Second, AM1710 was injected unilaterally in a single paw, whereas the entire lumbar enlargement (ie, ipsilateral and contralateral to intraplantar injection) was used in qPCR analysis. Third, the time point to collect the tissue differed between these 2 studies (ie, 45 minutes after intraplantar injection in this study vs 30 minutes after i.p injection in the prior study[21]). MCP-1 was decreased at 30 minutes within the dorsal horn of the spinal cord after i.p injection of AM1710 in the CCI model, indicating it is an early modulator in the mechanisms of reversal of neuropathic pain.[94] The increase in the TNF-α mRNA level observed here in the lumbar spinal cord after intraplantar AM1710 compared with vehicle treatment was unexpected and may reflect compensatory changes. More work is needed to better understand the role of TNF-α in the antiallodynic effects by CB_2 agonists and how CB_2 agonists impact the time course of changes in cytokines and chemokines during the development and maintenance of CIPN.

As shown in **Figure 10**, keratinocytes are replaced from progenitor cells at the deepest layer, SB. From SB, nascent keratinocytes are displaced superficially and undergo a stratified differentiation through SS and SG. During this progression,

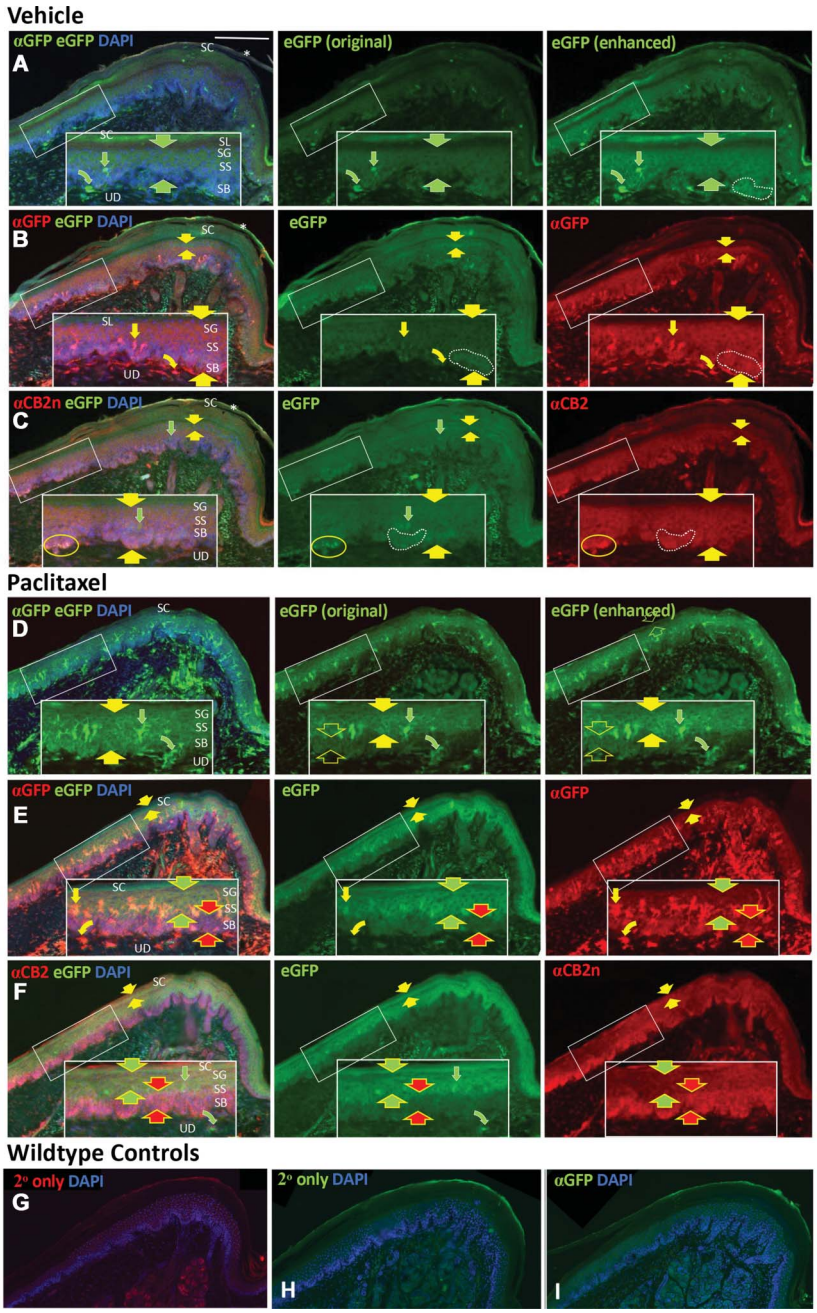

Figure 10. CB_2 immunolabeling is detected among epidermal keratinocytes and LCs in distal volar pads of hind paw plantar glabrous skin from CB_2^{EGFP} mice. Sequential sections are labeled for anti-GFP protein (GFP) or anti- CB_2 n-terminal domain (CB_2R_{nt}), and nuclei are counterstained with DAPI (blue fluorescence). Scale bar in upper left image = 100 μm. Inserts in white rectangles are 2X magnifications of locations in the smaller white rectangles. The layers of skin assessed are the upper dermis (UD) and the epidermis consisting from deep to superficial of stratum basalis (SB), stratum spinosum (SS), stratum granulosum (SG), stratum lucidum (SL), and stratum corneum (SC). Rows A–C: sequential sections from a mouse treated with vehicle; rows D–F: sequential sections from a mouse treated with paclitaxel. Rows A, D: endogenous EGFP fluorescence which is augmented by green fluorescence using immunolabeling with GFP primary antibody and secondary antibody conjugated with Alexa488. The left image in each row shows immunolabeling for GFP-Alexa488, endogenous EGFP, and DAPI. The middle image of each row depicts the relatively weak original endogenous EGFP fluorescence ($EGFP_{oe}$) captured before the section was immunolabeled using the identical camera settings used for GFP Alexa-488 as shown in the left images. The right image in each row is a copy of the original EGFP fluorescence capture that has been digitally enhanced ($EGFP_{de}$) to a level comparable with that of the GFP-Alexa488. The same level of digital enhancement of endogenous EGFP fluorescence was used for the left and middle images in rows B, C, E, and F. Rows B and E: The left images in each row are the combined immunolabeling for GFP with Cy3-conjugated secondary antibody (red), $EGFP_{de}$ (green), and DAPI (blue). Middle images are only the $EGFP_{de}$, right images only GFP-Cy3. Rows C, F: The left images in each row are the combined labeling for CB_2R_{nt} with Cy3-conjugated secondary antibody (red), $EGFP_{de}$ (green), and DAPI (blue). Middle images show only the enhanced $EGFP_{de}$, right images only CB_2R_{nt}-Cy3. All rows: Broad arrows are used in pairs to bracket the fluorescent signals of endogenous EGFP, or immunolabeling for GFP, and CB_2R_{nt} among strata of epidermal keratinocytes. Curved arrows indicate presumptive dendritic cells in the dermis, and straight arrows indicate LCs. Yellow arrows indicate double labeling for the particular combination within each row of images; red and green arrows indicate single labeling. G, H, I. Images from wildtype hind paw specimens. The sections in G and H were processed with the primary antibodies omitted and only with the secondary antibodies used in this study and DAPI: G, donkey anti-rabbit Cy3; and H. donkey anti-rabbit Alexa488. The section in **I** was processed with rabbit anti-GFP and donkey anti-rabbit Alexa 488. Samples were derived from mice perfused 16 days after initiation of paclitaxel dosing as described in Methods. EGFP, enhanced green fluorescent protein; GFP, green fluorescent protein; LC, Langerhans cells.

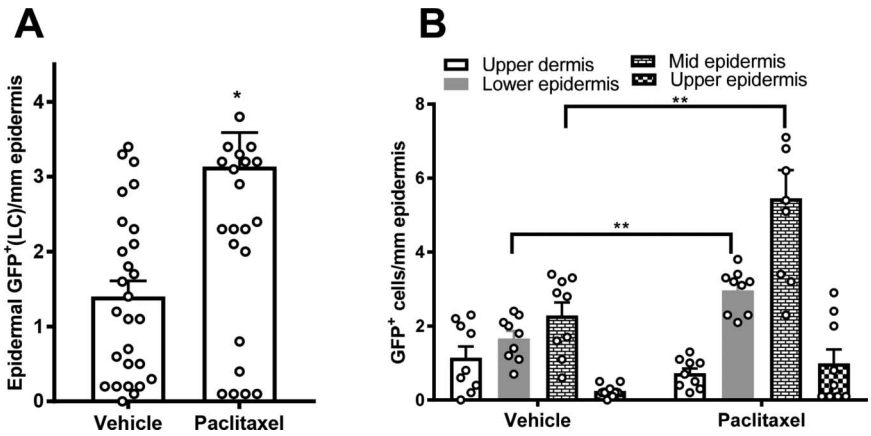

Figure 11. Paclitaxel treatment increased GFP signal among epidermal Langerhans cells (LCs). (A) Total epidermal LCs counts were increased among the paclitaxel-treated group compared with cremophor-vehicle treatment. (B) Location breakouts of the total GFP dermal dendritic cell and epidermal LCs populations. $^{*}P < 0.05$ vs vehicle treatment; $^{**}P < 0.01$ vehicle treatment vs corresponding paclitaxel treatment, unpaired 2 sample *t* test. Samples were derived from mice perfused 16 days after initiation of paclitaxel dosing as described in Methods. GFP, green fluorescent protein; LC, Langerhans cell.

keratinocytes become increasingly keratinized and lipid rich, referred to as the stratum lucidum (SL). Keratinocytes complete this transformation to subsequently become completely keratinized in forming a dead physically protective layer, SC. Although the keratinocytes of SC are dead, they can still contain varying degrees of previously functional residual proteins (eg, **Figs. 10C and F**).

Ample evidence supports a role for keratinocytes, Merkel cells, and LCs in mediating various aspects of normal sensation or pain sensitivity. A variety of neurosignaling molecules are expressed in keratinocytes in stratified patterns that are altered in human chronic afflictions and in experimental animal models of induced pain.[22,37,41,44,46,98] These observations suggest that keratinocytes play a role in modulating the sensitivity of normal nociceptive and nonnociceptive sensory endings located in or near the epidermis and may contribute to acute and chronic pain under pathological conditions. Recent optogenetic models confirm that stimulation limited to keratinocytes could modulate and initiate nociception or antinociception-related responses.[6,63,68] Consistent with a prior study suggesting the presence of CB_2 immunreactivity among keratinocytes in normal skin,[41] GFP reporter immunolabeling was detected in keratinocytes that coexpressed immunolabeling for GFP and CB_2 protein in our CB_2^{EGFP} mice. Moreover, the pattern of distribution of these 3 markers was substantially altered by paclitaxel treatment. However, paclitaxel did not reliably alter paw skin CB_2 or GFP mRNA levels by quantitative RT-PCR (**Figs. 2C and F**). RNAscope may offer greater sensitivity to detect mRNA changes

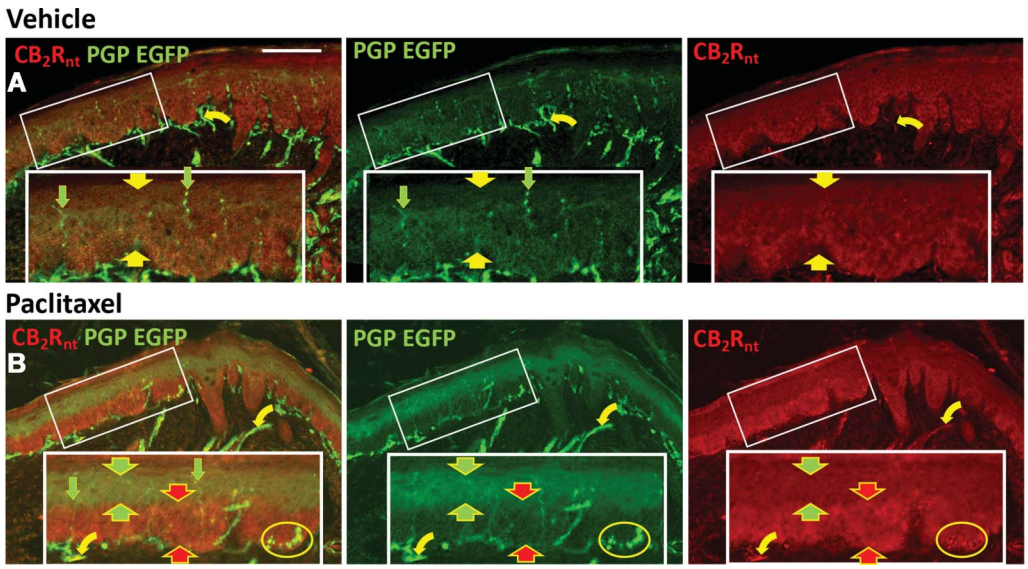

Figure 12. CB_2 Cy3 (red) and PGP9.5 Alexa488 (green) immunolabeling among epidermal keratinocytes and cutaneous innervation in sections from distal volar pads of hind paw plantar glabrous skin from CB_2^{EGFP} mice. Endogenous EGFP is coexpressed among the PGP9.5 Alexa 488 labeling. Scale bar in upper left image = 100 μm. Inserts in white rectangles are 2X magnifications of locations in the smaller white rectangles. Row A: sections from a mouse treated with vehicle; row B: sections from a mouse treated with paclitaxel. Yellow symbols indicate double labeling for the particular combination within each row of images; red and green arrows indicate single labeling. Broad arrows are used in pairs to bracket the expression of EGFP and labeling for CB_2R_{nt} among strata of epidermal keratinocytes. Straight arrows indicate sensory endings in the epidermis, and curved arrows indicate small nerves in the dermis. Samples were derived from mice perfused 16 days after initiation of paclitaxel dosing as described in Methods. EGFP, enhanced green fluorescent protein; PGP, protein gene product.

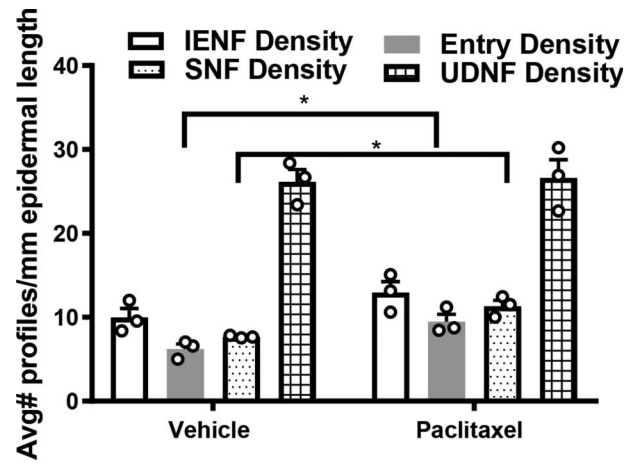

Figure 13. Quantification of innervation densities for intraepidermal nerve fibers (IENF), epidermal entry points, subepidermal nerve fibers (SNF), and upper dermal nerve fibers (UDNF) in paclitaxel-treated and vehicle-treated mice. $^*P < 0.05$ vehicle treatment vs corresponding paclitaxel treatment, unpaired 2-sample *t* test. Samples were derived from mice perfused 16 days after initiation of paclitaxel dosing as described in Methods.

in specific cell types compared with quantitative RT-PCR. The present observations are important because many CB_2 antibodies used previously in such localization studies also typically label in CB_2KO mice making interpretation of signal specificity problematic.[5,59] Given that available CB_2KO are functional (rather than complete) knockouts, use of a KO control to verify antibody specificity remains problematic and must be resolved in future studies using multiple antibodies directed at distinct epitopes that, in fact, correspond to the deletion site of the KO.

Activation of peripheral CB_2 in keratinocytes by a CB_2 agonist has been postulated to release the endogenous opioid peptide β-endorphin from keratinocytes.[28,41,43] However, another study indicated the antinociceptive effects of the CB_2 agonist AM1241 was not blocked by naloxone and likely independent of endogenous opioid systems in rats.[76] Strikingly, robust EGFP and CB_2 expression was detected on Merkel cells in the SB of the epidermis where they produce neuromodulatory effects on low-threshold mechanoreceptive Merkel endings supplied by myelinated Aβ DRG neurons that might contribute to mechanical allodynia under pathological conditions.[1,30]

The increased density of epidermal LCs in various pain conditions[16,18,47] suggests a possible neuroimmune communication between LCs and nerves in the pathogenesis of neuropathy.[51,81] The onset of pain triggered by an increase of LCs occurs by release of nitric oxide,[72] neurotrophic factors,[92] and proinflammatory cytokines,[20,81] resulting in the sensitization of nociceptors and mechanical hypersensitivity. In our study, the increase of GFP signals in LCs supports CB_2 involvement in the pathogenesis of neuropathy. The modulation of CB_2-mediated peripheral pathways could expand the potential utility of CB_2 as a therapeutic target.

Our PGP9.5 immunolabeling results confirmed that likely nociceptive innervation in and adjacent to the epidermis was present in both the vehicle-treated and paclitaxel-treated specimens; the failure to observe a loss of PGP9.5 innervation may reflect the dose of paclitaxel used but is consistent with observations by the Integrated Tissue Dynamics group in both clinical and preclinical samples. Importantly, a definitive expression of EGFP or GFP protein was not detected among the sensory endings like that detected previously in other mouse lines using other molecularly driven GFP reporter constructs.[25,56,96]

It is critically important to align the therapeutic target with the appropriate clinical indication if we are to enhance prospects for successful clinical translation. We are unaware of any double blind crossover human CIPN study that identified what the potential pathological endpoint looked like in the specific clinical trial subjects before initiating the trial. Patient biopsies could be used to preselect patients most likely to respond to CB_2 agonist treatment based on alignment with the rodent data.

In conclusion, our results support a peripheral cannabinoid CB_2 mechanism for suppression of paclitaxel-induced neuropathy. We demonstrate localization and upregulation of anti-GFP immunolabeling on keratinocytes and LCs in the epidermis of the mouse volar pad after paclitaxel treatment. Our results identify potential peripheral targets for CB_2 agonists in suppressing CIPN and provide a rationale for peripherally restricted or topical treatments for neuropathic pain that engages these peripheral mechanisms.

Conflict of interest statement

B. Ruggiero, M. Dockum, G. Houk, P.J. Albrecht, and F.L. Rice are employed at Integrated Tissue Dynamics LLC. P.J. Albrecht and F.L. Rice also have adjunct appointments from SUNY Albany. The remaining authors have no conflicts of interest to declare.

Acknowledgements

The authors thank Gabriela Rajic and Romario Pacheco for expert technical assistance with sample crysectioning.
This work was supported by the National Institutes of Health National Institute on Drug Abuse (NIDA) [Grants DA047858, DA041229 and DA042584 (A.G.H. and K.M.) and the National Cancer Institute [Grant CA200417 (A.G.H.)], an Indiana Addiction Grand Challenge Grant (A.G.H.), the Research and Education Component of the Advancing a Healthier Wisconsin Endowment at the Medical College of Wisconsin (C.J.H), and the Ministerio de Economía y Competitividad (SAF 2016-75959-R and SAF PID2019-108992RB-I00 to JR). L.M.C. was supported by T32 NIDA training grant DA024628 and the Harlan Scholars Research Program.

Appendix A. Supplemental digital content

Supplemental digital content associated with this article can be found online at http://links.lww.com/PAIN/B516.

Article history:
Received 10 February 2021
Received in revised form 13 September 2021
Accepted 15 September 2021
Available online 24 September 2021

References

[1] Abraham J, Mathew S. Merkel cells: a collective review of current concepts. Int J Appl Basic Med Res 2019;9:9–13.
[2] An D, Peigneur S, Hendrickx LA, Tytgat J. Targeting cannabinoid receptors: current status and prospects of natural products. Int J Mol Sci 2020;21:1–33.
[3] Atwood BK, Mackie K. CB 2: a cannabinoid receptor with an identity crisis. Br J Pharmacol 2010;160:467–79.

[4] Austin PJ, Moalem-Taylor G. The neuro-immune balance in neuropathic pain: involvement of inflammatory immune cells, immune-like glial cells and cytokines. J Neuroimmunol 2010;229:26–50.
[5] Baek JH, Darlington CL, Smith PF, Ashton JC. Antibody testing for brain immunohistochemistry: brain immunolabeling for the cannabinoid CB2 receptor. J Neurosci Methods 2013;216:87–95.
[6] Baumbauer KM, Deberry JJ, Adelman PC, Miller RH, Hachisuka J, Lee KH, Ross SE, Koerber HR, Davis BM, Albers KM. Keratinocytes can modulate and directly initiate nociceptive responses. Elife 2015;4:1–14.
[7] Beltramo M, Bernardini N, Bertorelli R, Campanella M, Nicolussi E, Fredduzzi S, Reggiani A. CB2 receptor-mediated antihyperalgesia: possible direct involvement of neural mechanisms. Eur J Neurosci 2006;23:1530–8.
[8] Benito C, Castillo AI, Romero J, Tolón RM, Núñez E, Pazos MR. Cannabinoid CB 2 receptors in human brain inflammation . Br J Pharmacol 2007;153:277–85.
[9] Benito C, Núñez E, Tolón RM, Carrier EJ, Rábano A, Hillard CJ, Romero J. Cannabinoid CB2 receptors and fatty acid amide hydrolase are selectively overexpressed in neuritic plaque-associated glia in Alzheimer's disease brains. J Neurosci 2003;23:11136–41.
[10] Benito C, Romero JP, Tolón RM, Clemente D, Docagne F, Hillard CJ, Guaza C, Romero J. Cannabinoid CB1 and CB2 receptors and fatty acid amide hydrolase are specific markers of plaque cell subtypes in human multiple sclerosis. J Neurosci 2007;27:2396–402.
[11] Bouchard J, Truong J, Bouchard K, Dunkelberger D, Desrayaud S, Moussaoui S, Tabrizi SJ, Stella N, Muchowski PJ. Cannabinoid receptor 2 signaling in peripheral immune cells modulates disease onset and severity in mouse models of huntington's disease. J Neurosci 2012;32: 18259–68.
[12] Boyette-Davis J, Xin W, Zhang H, Dougherty PM. Intraepidermal nerve fiber loss corresponds to the development of Taxol-induced hyperalgesia and can be prevented by treatment with minocycline. PAIN 2011;152: 308–13.
[13] Brown SM, Wager-Miller J, Mackie K. Cloning and molecular characterization of the rat CB2 cannabinoid receptor. Biochim Biophys Acta - Gene Struct Expr 2002;1576:255–64.
[14] Carey L, Gutierrez T, Deng L, Lee W, Mackie K, Hohmann A. Inflammatory and neuropathic nociception is preserved in GPR55 knockout mice. Sci Rep 2017;7:1–14.
[15] Carozzi VA, Canta A, Chiorazzi A. Chemotherapy-induced peripheral neuropathy: what do we know about mechanisms?. Neurosci Lett 2015; 596:90–107.
[16] Casanova-Molla J, Morales M, Planas-Rigol E, Bosch A, Calvo M, Grau-Junyent JM, Valls-Solé J. Epidermal Langerhans cells in small fiber neuropathies. PAIN 2012;153:982–9.
[17] Clark AK, Old EA, Malcangio M. Neuropathic pain and cytokines: current perspectives. J Pain Res 2013;6:803–14.
[18] Dauch JR, Bender DE, Luna-Wong LA, Hsieh W, Yanik BM, Kelly ZA, Cheng HT. Neurogenic factor-induced Langerhans cell activation in diabetic mice with mechanical allodynia. J Neuroinflammation 2013;10: 1–10.
[19] Deng L, Cornett BL, Mackie K, Hohmann AG. CB1 knockout mice unveil sustained CB2-mediated antiallodynic effects of the mixed CB1/CB2 agonist CP55,940 in a mouse model of paclitaxel-induced neuropathic pain. Mol Pharmacol 2015;88:64–74.
[20] Deng L, Ding W, Granstein RD. Thalidomide inhibits tumor necrosis factor-α production and Antigen presentation by langerhans cells. J Invest Dermatol 2003;121:1060–5.
[21] Deng L, Guindon J, Cornett BL, Makriyannis A, Mackie K, Hohmann AG. Chronic cannabinoid receptor 2 activation reverses paclitaxel neuropathy without tolerance or cannabinoid receptor 1-dependent withdrawal. Biol Psychiatry 2015;77:475–87.
[22] Dussor G, Koerber HR, Oaklander AL, Rice FL, Molliver DC. Nucleotide signaling and cutaneous mechanisms of pain transduction. Brain Res Rev 2009;60:24–35.
[23] Ellert-Miklaszewska A, Grajkowska W, Gabrusiewicz K, Kaminska B, Konarska L. Distinctive pattern of cannabinoid receptor type II (CB2) expression in adult and pediatric brain tumors. Brain Res 2007;1137: 161–9.
[24] Ferris CF, Nodine S, Pottala T, Cai X, Knox TM, Fofana FH, Kim S, Kulkarni P, Crystal JD, Hohmann AG. Alterations in brain neurocircuitry following treatment with the chemotherapeutic agent paclitaxel in rats. Neurobiol Pain 2019;6:100034.
[25] Fünfschilling U, Ng YG, Zang K, Miyazaki JI, Reichardt LF, Rice FL. TrkC kinase expression in distinct subsets of cutaneous trigeminal innervation and nonneuronal cells. J Comp Neurol 2004;480:392–414.
[26] Gado F, Meini S, Bertini S, Digiacomo M, Macchia M, Manera C. Allosteric modulators targeting cannabinoid cb1 and cb2 receptors: implications for drug discovery. Future Med Chem 2019;11:2019–37.
[27] Galiègue S, Mary S, Marchand J, Dussossoy D, Carrière D, Carayon P, Bouaboula M, Shire D, LE Fur G, Casellas P. Expression of central and peripheral cannabinoid receptors in human immune tissues and leukocyte subpopulations. Eur J Biochem 1995;232:54–61.
[28] Gao F, Zhang L, Su T, Li L, Zhou R, Peng M, Wu C, Yuan X, Sun N, Meng X. Signaling mechanism of cannabinoid receptor-2 activation-induced β -endorphin release. Mol Neurobiol 2016;53:3616–25.
[29] Griffin G, Wray EJ, Tao Q, Mcallister SD, Rorrer WK, Aung M, Martin BR, Abood ME. Evaluation of the cannabinoid CB 2 receptor-selective antagonist , SR144528: further evidence for cannabinoid CB 2 receptor absence in the rat central nervous system. Eur J Pharmacol 1999;377: 117–25.
[30] Gu JG. Molecular mechanisms of the sense of touch: an overview of mechanical transduction and transmission in merkel discs of whisker hair follicles and some clinical perspectives. Adv Exp Med Biol 2018;1099: 1–12.
[31] Guindon J, Hohmann aG. Cannabinoid CB2 receptors: a therapeutic target for the treatment of inflammatory and neuropathic pain. Br J Pharmacol 2008;153:319–34.
[32] Gutierrez T, Farthing JN, Zvonok AM, Makriyannis A, Hohmann AG. Activation of peripheral cannabinoid CB 1 and CB 2 receptors suppresses the maintenance of inflammatory nociception: a comparative analysis. Br J Pharmacol 2007;150:153–63.
[33] Herkenham M, Lynn AB, Johnson MR, Melvin LS, De Costa BR, Rice KC. Characterization and localization of cannabinoid receptors in rat brain: a quantitative in vitro autoradiographic study. J Neurosci 1991;11:563–83.
[34] Hilliges M, Wang L, Johansson O. Ultrastructural evidence for nerve fibers within all vital layers of the human epidermis. J Invest Dermatol 1995;104: 134–7.
[35] Hohmann AG. Spinal and peripheral mechanisms of cannabinoid antinociception: behavioral, neurophysiological and neuroanatomical perspectives. Chemistry and Physics of Lipids. Chem Phys Lipids 2002;121:173–90.
[36] Hollinshead SP, Tidwell MW, Palmer J, Guidetti R, Sanderson A, Johnson MP, Chambers MG, Oskins J, Stratford R, Astles PC. Selective cannabinoid receptor type 2 (CB2) agonists: optimization of a series of purines leading to the identification of a clinical candidate for the treatment of osteoarthritic pain. J Med Chem 2013;56:5722–33.
[37] Hou Q, Barr T, Gee L, Vickers J, Wymer J, Borsani E, Rodella L, Getsios S, Burdo T, Eisenberg E, Guha U, Lavker R, Kessler J, Chittur S, Fiorino D, Rice F, Albrecht P. Keratinocyte expression of calcitonin gene-related peptide β: implications for neuropathic and inflammatory pain mechanisms. PAIN 2011;152:2036–51.
[38] Howlett AC, Barth F, Bonner TI, Cabral G, Casellas P, Devane WA, Felder CC, Herkenham M, Mackie K, Martin BR, Mechoulam R, Pertwee RG. International union of pharmacology. XXVII. Classification of cannabinoid receptors. Pharmacol Rev 2002;54:161–202.
[39] Hung AL, Lim M, Doshi TL. Targeting cytokines for treatment of neuropathic pain. Scand J Pain 2017;17:287–93.
[40] Ibrahim MM, Deng H, Zvonok A, Cockayne DA, Kwan J, Mata HP, Vanderah TW, Lai J, Porreca F, Makriyannis A, Malan TP. Activation of CB2 cannabinoid receptors by AM1241 inhibits experimental neuropathic pain: pain inhibition by receptors not present in the CNS. Proc Natl Acad Sci U S A 2003;100:10529–33.
[41] Ibrahim MM, Porreca F, Lai J, Albrecht PJ, Rice FL, Khodorova A, Davar G, Makriyannis A, Vanderah TW, Mata HP, Malan TP. CB2 cannabinoid receptor activation produces antinociception by stimulating peripheral release of endogenous opioids. Proc Natl Acad Sci 2005;102:3093–8.
[42] Iyer V, Slivicki RA, Thomaz AC, Crystal JD, Mackie K, Hohmann AG. The cannabinoid CB2 receptor agonist LY2828360 synergizes with morphine to suppress neuropathic nociception and attenuates morphine reward and physical dependence. Eur J Pharmacol 2020;886:173544.
[43] Katsuyama S, Mizoguchi H, Kuwahata H, Komatsu T, Nagaoka K, Nakamura H, Bagetta G. Involvement of peripheral cannabinoid and opioid receptors in b -caryophyllene-induced antinociception. 2013;17: 664–75.
[44] Khodorova A, Navarro B, Jouaville LS, Murphy JE, Rice FL, Mazurkiewicz JE, Long-Woodward D, Stoffel M, Strichartz GR, Yukhananov R, Davar G. Endothelin-B receptor activation triggers an endogenous analgesic cascade at sites of peripheral injury. Nat Med 2003;9:1055–61.
[45] Krukowski K, Eijkelkamp N, Laumet G, Hack CE, Li Y, Dougherty PM, Heijnen CJ, Kavelaars A. CD8+ T cells and endogenous IL-10 are required for resolution of chemotherapy-induced neuropathic pain. J Neurosci 2016;36:11074–83.

[46] Kwan KY, Glazer JM, Corey DP, Rice FL, Stucky CL. TRPA1 modulates mechanotransduction in cutaneous sensory neurons. J Neurosci 2009; 29:4808–19.
[47] Lauria G, Lombardi R, Camozzi F, Devigili G. Skin biopsy for the diagnosis of peripheral neuropathy. Histopathology 2009;54:273–85.
[48] Lee WH, Carey LM, Li LL, Xu Z, Lai YY, Courtney MJ, Hohmann AG. ZLc002, a putative small-molecule inhibitor of nNOS interaction withNOS1AP, suppresses inflammatory nociception and chemotherapy-induced neuropathicpain and synergizes with paclitaxel to reduce tumor cellviability. Mol Pain 2018;14:1744806918801224.
[49] Lee W, Li L, Chawla A, Hudmon A, Lai Y, Courtney M, Hohmann A. Disruption of nNOS-NOS1AP protein-protein interactions suppresses neuropathic pain in mice. PAIN 2018;159:849–63.
[50] Lee W, Xu Z, Ashpole N, Hudmon A, Kulkarni P, Thakur G, Lai Y, Hohmann A. Small molecule inhibitors of PSD95-nNOS protein-protein interactions as novel analgesics. Neuropharmacology 2015;97:464–75.
[51] Lees JG, Makker PGS, Tonkin RS, Abdulla M, Park SB, Goldstein D, Moalem-Taylor G. Immune-mediated processes implicated in chemotherapy-induced peripheral neuropathy. Eur J Cancer 2017;73: 22–9.
[52] Li AL, Lin X, Dhopeshwarkar AS, Thomaz AC, Carey LM, Liu Y, Nikas SP, Makriyannis A, Mackie K, Hohmann AG. Cannabinoid CB2 agonist AM1710 differentially suppresses distinct pathological pain states and attenuates morphine tolerance and withdrawal. Mol Pharmacol 2019;95: 155–68.
[53] Li Y, Kim J. CB2 cannabinoid receptor knockout in mice impairs contextual long-term memory and enhances spatial working memory. Neural Plast 2016;2016:9817089.
[54] Lin X, Dhopeshwarkar AS, Huibregtse M, MacKie K, Hohmann AG. Slowly signaling G protein-biased CB2 cannabinoid receptor agonist LY2828360 suppresses neuropathic pain with sustained efficacy and attenuates morphine tolerance and dependence. Mol Pharmacol 2018; 93:49–62.
[55] López A, Aparicio N, Pazos MR, Grande MT, Barreda-manso MA, Benito-cuesta I, Vázquez C, Amores M, Ruiz-pérez G, García-garcía E, Beatka M, Tolón RM, Dittel BN, Hillard CJ, Romero J. Cannabinoid CB 2 receptors in the mouse brain: relevance for Alzheimer ' s disease. J Neuroinflammation 2018;15:158.
[56] Luo W, Enomoto H, Rice FL, Milbrandt J, Ginty DD. Molecular identification of rapidly Adapting mechanoreceptors and their developmental dependence on ret signaling. Neuron 2009;64:841–56.
[57] Malan TP, Ibrahim MM, Deng H, Liu Q, Mata HP, Vanderah T, Porreca F, Makriyannis A. CB2 cannabinoid receptor-mediated peripheral antinociception. PAIN 2001;93:239–45.
[58] Mancarci BO, Toker L, Tripathy SJ, Li B, Rocco B, Sibille E, Pavlidis P. Cross-laboratory analysis of brain cell type transcriptomes with applications to interpretation of bulk tissue data. eNeuro 2017;4: ENEURO.0212-17.2017.
[59] Marchalant Y, Brownjohn PW, Bonnet A, Kleffmann T, Ashton JC. Validating antibodies to the cannabinoid CB2 receptor: antibody sensitivity is not evidence of antibody specificity. J Histochem Cytochem 2014;62:395–404.
[60] Di Marzo V, Melck D, Bisogno T, De Petrocellis L. Endocannabinoids: endogenous cannabinoid receptor ligands with neuromodulatory action. Trends Neurosci 1998;21:521–8.
[61] Miaskowski C, Mastick J, Paul SM, Abrams G, Cheung S, Sabes JH, Kober KM, Schumacher M, Conley YP, Topp K, Smoot B, Mausisa G, Mazor M, Wallhagen M, Levine JD. Impact of chemotherapy-induced neurotoxicities on adult cancer survivors' symptom burden and quality of life. J Cancer Surviv 2018;12:234–45.
[62] Milligan ED, Penzkover KR, Soderquist RG, Mahoney MJ. Spinal interleukin-10 therapy to treat peripheral neuropathic pain. Neuromodulation 2012;15:520–6.
[63] Moehring F, Cowie AM, Menzel AD, Weyer AD, Grzybowski M, Arzua T, Geurts AM, Palygin O, Stucky CL. Keratinocytes mediate innocuous and noxious touch via ATP-P2X4 signaling. Elife 2018;7:e31684.
[64] Morales P, Hernandez-Folgado L, Goya P, Jagerovic N. Cannabinoid receptor 2 (CB2) agonists and antagonists: a patent update. Expert Opin Ther Pat 2016;26:843–56.
[65] Moreira FA, Grieb M, Lutz B. Central side-effects of therapies based on CB1 cannabinoid receptor agonists and antagonists: focus on anxiety and depression. Best Pract Res Clin Endocrinol Metab 2009;23:133–44.
[66] Munro S, Thomas KL, Shaar MA, Abu-Shaar M. Molecular characterization of a peripheral receptor for cannabinoids. Nature 1993; 365:61–5.
[67] Nent E, Nozaki C, Schmöle AC, Otte D, Zimmer A. CB2 receptor deletion on myeloid cells enhanced mechanical allodynia in a mouse model of neuropathic pain. Sci Rep 2019;9:1–11.
[68] Pang Z, Sakamoto T, Tiwari V, Kim YS, Yang F, Dong X, Güler AD, Guan Y, Caterina MJ. Selective keratinocyte stimulation is sufficient to evoke nociception in mice. PAIN 2015;156:656–65.
[69] Pereira A, Chappell A, Dethy J, Hoeck H, Arendt-Nielsen L, Verfaille S, Boulanger B, Jullion A, Johnson M, McNearney T. A proof-of concept (poc study including experimental pain models (epms) to assess the effects of a CB2 agonist (LY2828360) in the treatment of patients with osteoarthritic (OA) knee pain. Clin Pharmacol Ther 2013;93:S56–7. No. PII-11.
[70] Petersen K, Rice F, Farhadi M, Reda H, Rowbotham M. Natural history of cutaneous innervation following herpes zoster. PAIN 2010;150:75–82.
[71] Petersen K, Rice F, Suess F, Berro M, Rowbotham M. Relief of post-herpetic neuralgia by surgical removal of painful skin. PAIN 2002;98: 119–26.
[72] Qureshi AA, Hosoi J, Xu S, Takashima A, Granstein RD, Lerner EA. Langerhans cells express inducible nitric oxide synthase and produce nitric oxide. J Invest Dermatol 1996;107:815–21.
[73] Rahn EJ, Deng L, Thakur GA, Vemuri K, Zvonok AM, Lai YY, Makriyannis A, Hohmann AG. Prophylactic cannabinoid administration blocks the development of paclitaxel-induced neuropathic nociception during analgesic treatment and following cessation of drug delivery. Mol Pain 2014;10:27.
[74] Rahn EJ, Hohmann AG. Cannabinoids as pharmacotherapies for neuropathic pain: from the bench to the bedside. Neurotherapeutics 2009;6:713–37.
[75] Rahn EJ, Thakur GA, Wood JAT, Zvonok AM, Makriyannis A, Hohmann AG. Pharmacological characterization of AM1710, a putative cannabinoid CB2agonist from the cannabilactone class: antinociception without central nervous system side-effects. Pharmacol Biochem Behav 2011;98:493–502.
[76] Rahn EJ, Zvonok AM, Makriyannis A, Hohmann AG. Antinociceptive effects of racemic AM1241 and its chirally synthesized enantiomers: lack of dependence upon opioid receptor activation. AAPS J 2010;12: 147–57.
[77] Rahn EJ, Zvonok AM, Thakur Ga, Khanolkar AD, Makriyannis A, Hohmann AG. Selective activation of cannabinoid CB2 receptors suppresses neuropathic nociception induced by treatment with the chemotherapeutic agent paclitaxel in rats. J Pharmacol Exp Ther 2008; 327:584–91.
[78] Rice FL, Castel D, Ruggiero E, Dockum M, Houk G, Sabbag I, Albrecht PJ, Meilin S. Human-like cutaneous neuropathologies associated with a porcine model of peripheral neuritis: a translational platform for neuropathic pain. Neurobiol Pain 2019;5:100021.
[79] Saroz Y, Kho DT, Glass M, Graham ES, Grimsey NL. Cannabinoid receptor 2 (CB2) signals via G-alpha-s and induces IL-6 and IL-10 cytokine secretion in human primary leukocytes. ACS Pharmacol Transl Sci 2019;2:414–28.
[80] Schmöle AC, Lundt R, Gennequin B, Schrage H, Beins E, Krämer A, Zimmer T, Limmer A, Zimmer A, Otte DM. Expression analysis of CB2-GFP BAC transgenic mice. PLoS One 2015;10:1–16.
[81] Siau C, Xiao W, Bennett GJ. Paclitaxel- and vincristine-evoked painful peripheral neuropathies: loss of epidermal innervation and activation of Langerhans cells. Exp Neurol 2006;201:507–14.
[82] Sibaud V, Leboeuf NR, Roche H, Belum VR, Gladieff L, Deslandres M, Montastruc M, Eche A, Vigarios E, Dalenc F, Lacouture ME. Dermatological adverse events with taxane chemotherapy. Eur J Dermatol 2016;26:427–43.
[83] Slivicki R, Ali Y, Lu H, Hohmann A. Impact of genetic reduction of NMNAT2 on chemotherapy-induced losses in cell viability in vitro and peripheral neuropathy in vivo. PLoS One 2016;11:e0147620.
[84] Slivicki R, Xu Z, Mali S, Hohmann A. Brain permeant and impermeant inhibitors of fatty-acid amide hydrolase suppress the development and maintenance of paclitaxel-induced neuropathic pain without producing tolerance or physical dependence in vivo and synergize with paclitaxel to reduce tumor. Pharmacol Res 2019;142:267–82.
[85] Slivicki RA, Iyer V, Mali SS, Garai S, Thakur GA, Crystal JD, Hohmann AG. Positive Allosteric modulation of CB1 cannabinoid receptor signaling enhances morphine antinociception and attenuates morphine tolerance without enhancing morphine- induced dependence or reward. Front Mol Neurosci 2020;0:54.
[86] Slivicki RA, Mali SS, Hohmann AG. Voluntary exercise reduces both chemotherapy-induced neuropathic nociception and deficits in hippocampal cellular proliferation in a mouse model of paclitaxel-induced peripheral neuropathy. Neurobiol Pain 2019;6:100035.
[87] Slivicki RA, Saberi SA, Iyer V, Vemuri VK, Makriyannis A, Hohmann AG. Brain-permeant and -impermeant inhibitors of fatty acid amide hydrolase synergize with the opioid analgesic morphine to suppress chemotherapy-

induced neuropathic nociception without enhancing effects of morphine on gastrointestinal transit. J Pharmacol Exp Ther 2018;367:551–63.
[88] Slivicki RA, Xu Z, Kulkarni PM, Pertwee RG, Mackie K, Thakur GA, Hohmann AG. Positive Allosteric modulation of cannabinoid receptor type 1 suppresses pathological pain without producing tolerance or dependence. Biol Psychiatry 2018;84:722–33.
[89] Ständer S, Schmelz M, Metze D, Luger T, Rukwied R. Distribution of cannabinoid receptor 1 (CB1) and 2 (CB2) on sensory nerve fibers and adnexal structures in human skin. J Dermatol Sci 2005;38:177–88.
[90] Svíženská IH, Brázda V, Klusáková I, Dubový P. Bilateral changes of cannabinoid receptor type 2 protein and mRNA in the dorsal root ganglia of a rat neuropathic pain model. J Histochem Cytochem 2013;61:529–47.
[91] Thacker MA, Clark AK, Marchand F, McMahon SB. Pathophysiology of peripheral neuropathic pain: immune cells and molecules. Anesth Analg 2007;105:838–47.
[92] Torii H, Yan Z, Hosoi J, Granstein RD. Expression of neurotrophic factors and neuropeptide receptors by langerhans cells and the Langerhans cell-like cell line XS52: further support for a functional relationship between Langerhans cells and epidermal nerves. J Invest Dermatol 1997;109:586–91.
[93] Tsou K, Brown S, Sañudo-Peña MC, Mackie K, Walker JM. Immunohistochemical distribution of cannabinoid CB1 receptors in the rat central nervous system. Neuroscience 1998;83:393–411.
[94] Wilkerson JL, Alberti LB, Kerwin AA, Ledent CA, Thakur GA, Makriyannis A, Milligan ED. Peripheral versus central mechanisms of the cannabinoid type 2 receptor agonist AM1710 in a mouse model of neuropathic pain. Brain Behav 2020;10:e01850.
[95] Wotherspoon G, Fox A, McIntyre P, Colley S, Bevan S, Winter J. Peripheral nerve injury induces cannabinoid receptor 2 protein expression in rat sensory neurons. Neuroscience 2005;135:235–45.
[96] Yu H, Pan B, Weyer A, Wu HE, Meng J, Fischer G, Vilceanu D, Light AR, Stucky C, Rice FL, Hudmon A, Hogan Q. CaMKII controls whether touch is painful. J Neurosci 2015;35:14086–102.
[97] Zeisel A, Hochgerner H, Lönnerberg P, Johnsson A, Memic F, van der Zwan J, Häring M, Braun E, Borm LE, La Manno G, Codeluppi S, Furlan A, Lee K, Skene N, Harris KD, Hjerling-Leffler J, Arenas E, Ernfors P, Marklund U, Linnarsson S. Molecular architecture of the mouse nervous system. Cell 2018;174:999–1014.e22.
[98] Zhao P, Barr TP, Hou Q, Dib-Hajj SD, Black JA, Albrecht PJ, Petersen K, Eisenberg E, Wymer JP, Rice FL, Waxman SG. Voltage-gated sodium channel expression in rat and human epidermal keratinocytes: evidence for a role in pain. PAIN 2008;139:90–105.
[99] Zimmermann M. Ethical guidelines for investigations of experimental pain in conscious animals. PAIN 1983;16:109–10.